RESEARCH ARTICLE

Basin Research

IAS EAGE WILEY

The role of mantle upwelling on the thermal history of the Tertiary-Piedmont Basin at the Alps-Apennines tectonic boundary

Chiara Amadori[1] | Matteo Maino[1,2] | Mattia Marini[3] | Leonardo Casini[4] | Barbara Carrapa[5] | Gilby Jepson[5] | Robert George Hayes[5] | Chiara Nicola[1] | Simone Reguzzi[3] | Andrea Di Giulio[1]

[1]Department of Earth and Environmental Sciences, University of Pavia, Pavia, Italy

[2]Istituto di Geoscienze e Georisorse – Consiglio Nazionale Ricerce U.O.S. – Pavia, Pavia, Italy

[3]Department of Earth Science 'A. Desio', University of Milan, Milan, Italy

[4]Department of Chemistry, Physics, Mathematics and Natural Sciences, University of Sassari, Sassari, Italy

[5]Department of Geosciences, University of Arizona, Tucson, Arizona, USA

Correspondence
Matteo Maino, Department of Earth and Environmental Sciences, University of Pavia, Pavia, Italy.
Email: matteo.maino@unipv.it

Abstract

The Tertiary-Piedmont Basin (NW Italy) is an episutural basin that developed from the late Eocene on the Alps–Apennines tectonic junction. Several coeval geodynamic processes, including the loading and exhumation of the Western Alps, the outward migration of the Apennine accretionary wedge and the opening of the Liguro-Provençal rift basin, controlled the basin evolution. We integrate fluid-inclusion microthermometry, low-temperature thermochronology and burial history with numerical modelling to constrain the palaeo-geothermal gradients required and evaluate the mechanisms that governed the basin thermal history. Apatite fission-track and (U-Th-Sm)/He analyses of the basal late Eocene turbidites show reset ages of ca. 25 and 20 Ma, respectively, which require temperatures to be >120°C. Homogenization temperatures up to ca. 130°C from fluid inclusion analyses from authigenic minerals confirm the thermochronometric data, supporting a significant post-depositional heating in the lower sequence of the basin. Stratigraphic reconstructions and decompaction of the basin fill indicate that the maximum burial experienced by the basal strata at 25 Ma is 2.3 ± 0.1 km, which is not sufficient to reset the AFT thermochronometric system when applying a typical geothermal gradient (ca. 20–30°C/km). An elevated geothermal gradient of 45 ± 5°C/km is thus necessary to explain the thermochronometric dates and the elevated thermal signature at shallow depths. 2D numerical simulations indicate that such an elevated palaeo-geothermal gradient can be best explained by mantle upwelling, consistent with crustal thinning caused by the inception of the Liguro-Provençal rift basin and related outward migration of the Alpine and Apennine fronts during the Oligocene.

KEYWORDS

Alps-Apennines, apatite fission track, high geothermal gradient, mantle upwelling, Tertiary-Piedmont basin, thermal history, thermal modelling

1 | INTRODUCTION

The thermal evolution of sedimentary basins is important for our understanding of the tectonic history of orogenic systems (Allen & Allen, 2013; Armstrong, 2005; Ceriani et al., 2002, 2006; DeCelles & Giles, 1996; Green, Duddy, Gleadow, & Lovering, 1989; Jamieson et al., 1996; Osadetz et al., 2002). Basin subsidence is controlled by sedimentary, tectonic and thermal processes. The thermal structure of sedimentary basins is dominated by the basal heat flow, which is associated with variable lithospheric scale processes such as the thickness of the lithosphere, magmatic underplating and fluid circulation (Armstrong & Chapman, 1998; Di Giulio et al., 2021; Mangenot et al., 2017; Tamburelli et al., 2022; Yalçin et al., 1997; Yalçin & Welte, 1988). Significant and spatially extensive deviations from a steady-state thermal configuration are often difficult to detect in the basin due to the smoothing effect of heat diffusion in crustal rocks and the low thermal conductivity of the sedimentary rocks. Despite these challenges, constraining time-integrated thermal histories is crucial for understanding diagenetic processes, hydrocarbon generation and migrations, as well as large-scale tectonic and geodynamic processes (Ceriani et al., 2021; Corrado et al., 2020; Di Giulio et al., 2021; Gusmeo et al., 2021; Schneider & Issler, 2019). For instance, studies of sedimentary basins from the Alps (Mazurek et al., 2006) and Apennines (Cibin et al., 2003; Zattin et al., 2000) have shown how tectonic and magmatic processes can affect the burial history and result in multiple thermal events with diverse intensity, age, and duration that are difficult to disentangle.

Low-temperature (low-T) thermochronometry is a powerful tool to constrain the thermal history of rocks within the first ca. 10 km of the crust (e.g. <300°C; Reiners & Brandon, 2006). In fact, burial palaeotemperatures of sedimentary successions can be determined by apatite fission-track (AFT) and (U-Th-Sm)/He (AHe) thermochronology (Flowers et al., 2009; Gleadow et al., 1986). The combination of AFT and AHe techniques can be supported by other independent palaeo-thermometers, such as fluid-inclusion microthermometry (e.g. Goldstein & Reynolds, 1994), can constrain complex thermal histories.

In this contribution, we aim to reconstruct the thermal history of the Tertiary-Piedmont Basin (TPB hereafter; Figure 1), an episutural basin that experienced a complex tectono-sedimentary evolution due to its unique tectonic position above the junction of two orogenic systems with opposite vergence, that is, the Alps and the Apennines in the central Mediterranean. The tectonic evolution of the TPB is still highly debated; particularly elusive is the timing of compressional and extensional tectonics, and the timing of exhumation of the metamorphic rocks which provided sediments filling the basin (e.g.

Highlights

- Low-T thermochronology, fluid inclusion microthermometry and burial history constrain the Tertiary-Piedmont Basin thermal history.
- Basin experienced a post-depositional heating about 100°C at ca. 2 km of depth between 35 and 30 Ma.
- The Tertiary-Piedmont Basin recorded a palaeogeothermal gradient of ca. 45 ± 5°C/km.
- Thermal modelling indicates that heating is consistent with mantle upwelling.

Carrapa et al., 2003, 2016; Federico et al., 2007; Maino et al., 2012, 2013; Vignaroli et al., 2008, 2010). The primary mechanism suggested to explain the TPB subsidence evolution is lithospheric flexural loading induced by the Western Alps' load (Carrapa et al., 2016; Carrapa & Garcia-Castellanos, 2005). The subsidence and thermal history of the TPB were also influenced by the coeval rifting of the Liguro-Provençal basin and the northeastward shortening of the Northern Apennine (e.g. Bertotti et al., 2006; Carrapa et al., 2003; Maffione et al., 2008; Maino et al., 2013; Vignaroli et al., 2008). The study area is controlled by the complex dynamics of the Apennine and Alpine slabs, which are driven by processes such as roll back (Liu et al., 2022; Malusà et al., 2021; Salimbeni et al., 2021) and break-off (Carminati et al., 2012; Handy et al., 2010, 2021; Kästle et al., 2020; Schlunegger & Kissling, 2015; Vignaroli et al., 2008, 2010).

Due to its structural position atop the suture zone and multi-phase geodynamic evolution, the TPB provides an excellent case study for investigating regional- and lithospheric-scale processes. We present a multidisciplinary study applying low-T thermochronology (AFT and AHe) and fluid-inclusion microthermometry from a complete late Eocene–Miocene sequence to determine the thermal history of the basin. We combine thermochronological and geological constraints with finite-difference 2D numerical modelling to test among different heating mechanisms and the role of the deep mantle structure on the basin's thermal evolution.

2 | GEOLOGICAL BACKGROUND

2.1 | TPB setting in the Alps-Apennine evolution

The TPB developed from the late Eocene atop the tectonic fault zone separating the Alps to the west from
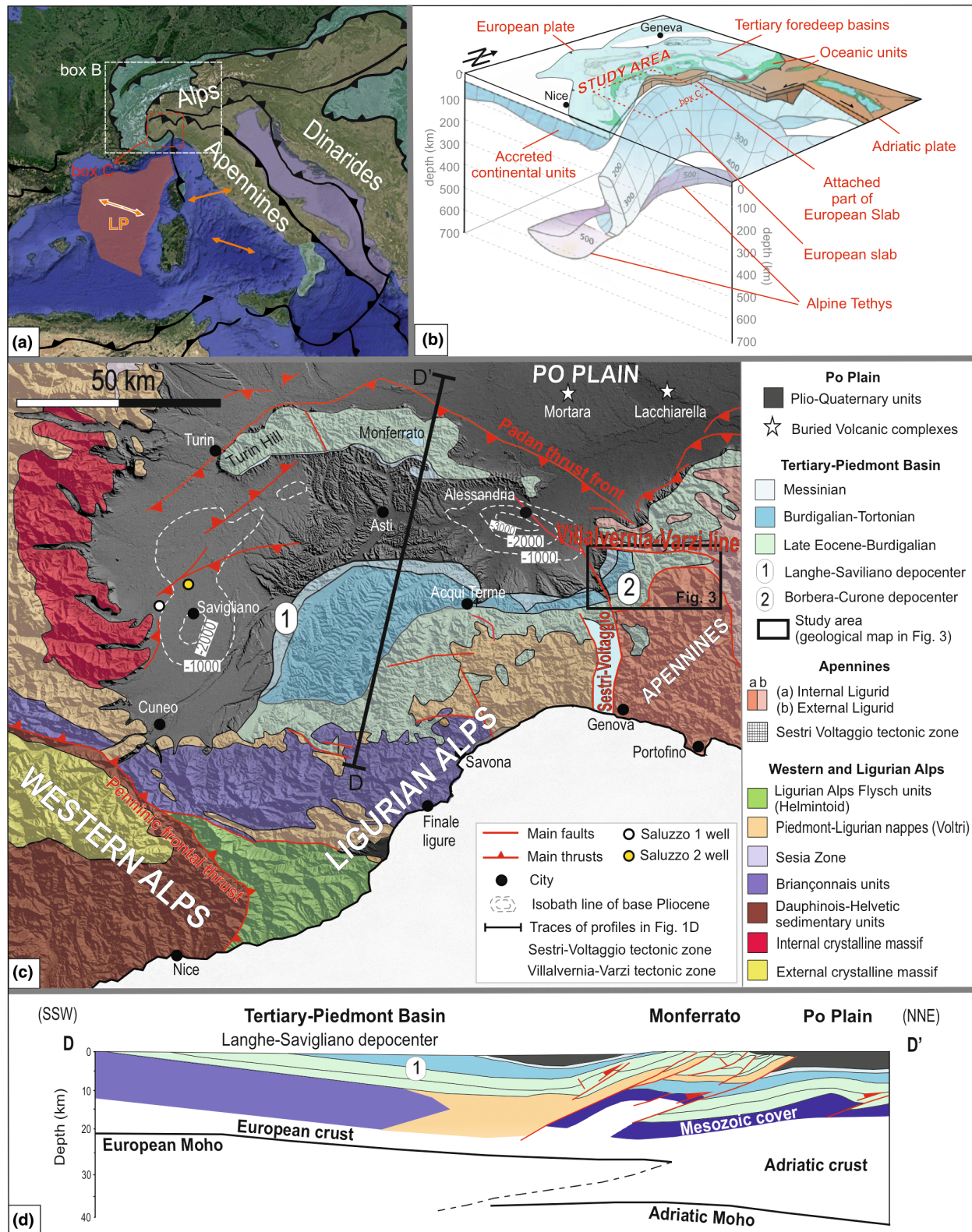
FIGURE 1 Geological and geodynamic setting of the study area. (a) Simplified geodynamic setting of the central Mediterranean area, modified after Capó and Garcia (2019) and Handy et al. (2021). Areas shaded in light blue correspond to the European plate, whereas those in light brown to the Adriatic plate. Orange arrows indicate the extended back-arc basins. LP indicates the Liguro-Provençal Basin. (b) 3D-sketch of the slab beneath the Alps as viewed from the southeast, modified from Handy et al. (2021). (c) Geological map of the Western and Ligurian Alps and Apennines (modified after Mosca et al., 2010 and Maino et al., 2013). Dashed grey lines are isobath (meters below sea level) of base Pliocene from Pieri and Groppi (1981) showing the Savigliano and Alessandria depocentres. (d) Geological profiles DD′ modified after Bertotti et al. (2006).

the Apennines to the east (Capponi et al., 2016; Crispini et al., 2009; Di Giulio & Galbiati, 1995; Laubscher et al., 1992; Maino et al., 2013; Mosca et al., 2010; Mutti et al., 1995). These two orogenic systems have opposite tectonic transport directions and are the result of the geodynamic evolution of three main continental plates—Africa, Adria, and Europe—and several interposed oceanic basins (Boccaletti et al., 1980; Castellarin, 2001; Jolivet & Faccenna, 2000; Trümpy, 1960; Vanossi et al., 1986). The TPB is bounded by: (i) metamorphic rocks of the Ligurian Alps to the south and southwest (Briançonnais units and Voltri massif; Figure 1), which experienced a complex, multi-stage deformation and metamorphic evolution (e.g. Bonini et al., 2010; Capponi & Crispini, 2002; Di Giulio et al., 2020; Federico et al., 2009; Maino et al., 2012, 2019; Maino & Seno, 2016; Mueller et al., 2020; Vignaroli et al., 2010); and (ii) Cretaceous low-grade metamorphic units, exposed to the east, which are part of the accretionary wedge of the Northern Apennines (Capponi et al., 2016; Marroni, Meneghini, & Pandolfi, 2010; Marroni, Ottria, & Pandolfi, 2010).

The Ligurian Alps (Figure 1) constitutes the southernmost segment of the Alpine belt and formed during the Cretaceous to Eocene southeastward subduction of the Piedmont-Ligurian Ocean underneath Adria, followed by the Oligocene Adria-Europe collision (e.g. Bonini et al., 2010; Capponi & Crispini, 2002; Rosenbaum & Lister, 2005; Vanossi et al., 1986).

Since the Oligocene, the Apennines belt experienced a ca. 50° counter-clockwise rotation, along with the entire Ligurian Alps-TPB system, around a pivot point located in the present-day Ligurian region (Laubscher et al., 1992; Maino et al., 2013; Vanossi et al., 1994). Apennine rotation was associated with extension of the Ligurian-Provençal rift basin (ca. 35–30 Ma; De Voogd et al., 1991; Rollet et al., 2002), with full oceanic spreading in the Miocene (Speranza et al., 2002). Rifting and consequent stretching of the lithosphere contributing to a high geothermal gradient were accompanied by the eastward drifting of the Corsica-Sardinia block (Gattacceca et al., 2007; Maffione et al., 2008). From the Late Miocene onwards, the tectonic evolution of the region is associated with the northeastward translation of the Apennine tectonic units carrying the TPB successions onto the Po Plain-Northern Adriatic foreland system (e.g. Amadori et al., 2019, 2020; Pieri & Groppi, 1981) (Figure 1d).

The TPB sedimentary sequence also records Oligocene-Miocene magmatism, evidenced by volcaniclastic deposits likely produced by volcanoes now relict in the western Po Plain subsurface (D'Atri et al., 2001; Di Giulio et al., 2001; Fantoni et al., 1999; Ruffini et al., 1995). This kind of volcanic activity in continental crust may be connected to magmatic underplating (Thybo & Artemieva, 2013), and will likely have disturbed the thermal state of the area.

The TPB is subdivided into a western sub-basin (Langhe), deposited entirely onto Alpine units, and a relatively smaller eastern sub-basin (Borbera-Curone), resting on top of the Apennine sedimentary units (Figure 1c). The Langhe are generally explained as representing the retro-foreland basin of the Western Alps (Carrapa et al., 2003, 2016; Carrapa & Garcia-Castellanos, 2005), whereas the eastern TPB is considered part of the Northern Apennines orogenic system (e.g. Di Giulio, 1991; Mutti et al., 1995; Ricci Lucchi, 1990).

2.2 | Stratigraphy of the TPB

The eastern TPB (Borbera-Curone sub-basin) accommodated a total of up to ca. 3 km of thick late Eocene-late Miocene deposits made of marginal marine to deep-water clastic sedimentary rocks (Andreoni et al., 1981; Cavanna et al., 1989; Di Giulio & Galbiati, 1995; Festa et al., 2015; Gelati, 1977; Gelati & Gnaccolini, 1978; Ghibaudo et al., 1985, 2019; Mutti et al., 1995; Rossi et al., 2009). This basin infill comprises multiple depositional sequences that have been interpreted to reflect major tectonic events (Di Giulio, 1991; Di Giulio et al., 2019; Mutti et al., 1995; Rossi & Craig, 2016) (Figure 2). The sedimentary fill of the eastern TPB begins with a late Eocene to earliest Oligocene regressive sequence comprising deep-water turbidites (Dernice and Grue turbiditic formations) and a few tens of meters of shelf to marginal-marine deposits (Rio Trebbio Sandstones Fm.) (Di Giulio, 1991). These deposits are unconformably overlain by late Rupelian deposits (Gelati, 1977), locally folded (Cavanna et al., 1989), suggesting syn-depositional late Eocene-late Rupelian compressional tectonics. The late Rupelian to Chattian depositional sequence initiates with >1200 m of fan delta conglomerates and coeval sand-rich turbidites (Savignone and Monastero Formations, respectively; Gelati, 1977) (Figure 3), which transition upwards into a few hundred of meters of slope hemipelagic marlstone (Gremiasco Fm.) embedding with coarse turbidites (Cavanna et al., 1989; Di Giulio & Galbiati, 1995; Marini et al., 2020). This sequence has been interpreted as recording the rapid uplift and the subsequent collapse of the Alpine edifice, which provided a high supply of relatively coarse clastic deposits followed by a relatively rapid regional-scale decrease in sediment supply (Di Giulio, 1991; Rossi & Craig, 2016). This rapid uplift may have also caused advection of the isotherms and therefore a thermal anomaly in the TPB.

Structural analyses (Festa et al., 2015; Marroni et al., 2002) and geometric relationships between the deposits suggest a late Chattian to early Aquitanian left-lateral transpressive activation of the Villavernia-Varzi tectonic line (Figure 1c; Di Giulio & Galbiati, 1995; Festa et al., 2015; Marroni et al., 2002). Continued deformation
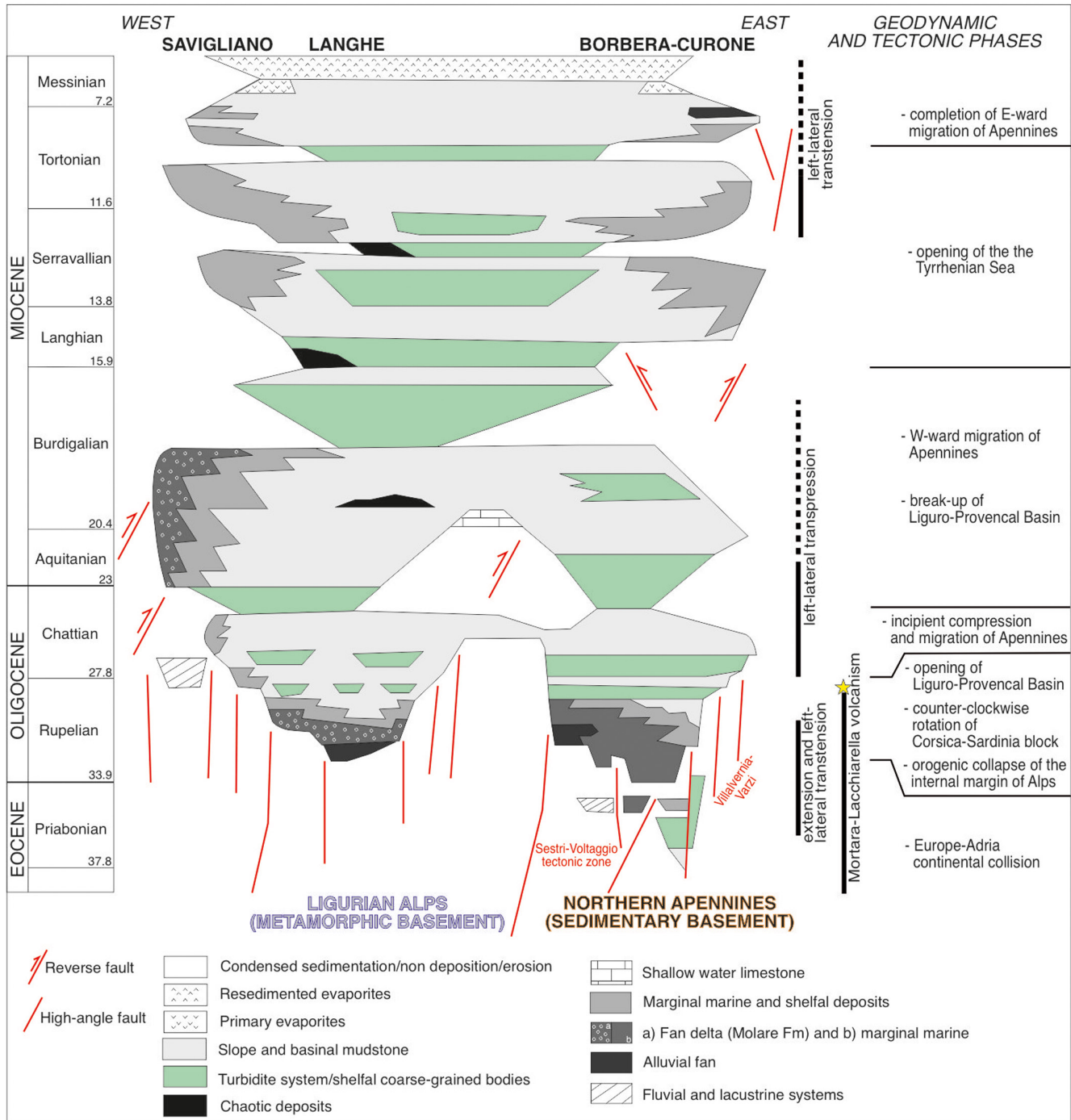
FIGURE 2 Stratigraphic and tectonic framework of the TPB. Chronostratigraphic scheme and deformation stages recorded in the whole TPB (after Di Giulio & Galbiati, 1995; Festa et al., 2015 and Rossi & Craig, 2016). Main tectonic and geodynamic events affecting the Alps-Apennines knot according to Maino et al. (2013). Yellow star: $^{40}Ar/^{39}Ar$ age (28.5 ± 0.1 Ma) of youngest volcanic rocks from Mortara 1 well, after Fantoni et al. (1999).

along this strike-slip fault resulted in a complex basin palaeogeography (Felletti, 2002), culminating in a relatively small, confined, turbidite-dominated basin (the Castagnola syncline; Stocchi et al., 1992; Felletti, 2004a,b). While sedimentation in the Castagnola depocentre is continuous throughout the early Miocene (Castagnola Fm.; Cavanna et al., 1989; Marini et al., 2016, 2020; Patacci

et al., 2020), the lower Miocene is missing in the western part of the study area (Figure 3a; Andreoni et al., 1981; Festa et al., 2015).

The stratigraphy of the western TPB (Langhe sub-basin) is described in several contributions (Ghibaudo et al., 2019; Maino et al., 2013; Rossi & Craig, 2016). The up to ca. 4 km thick clastic sequence unconformably
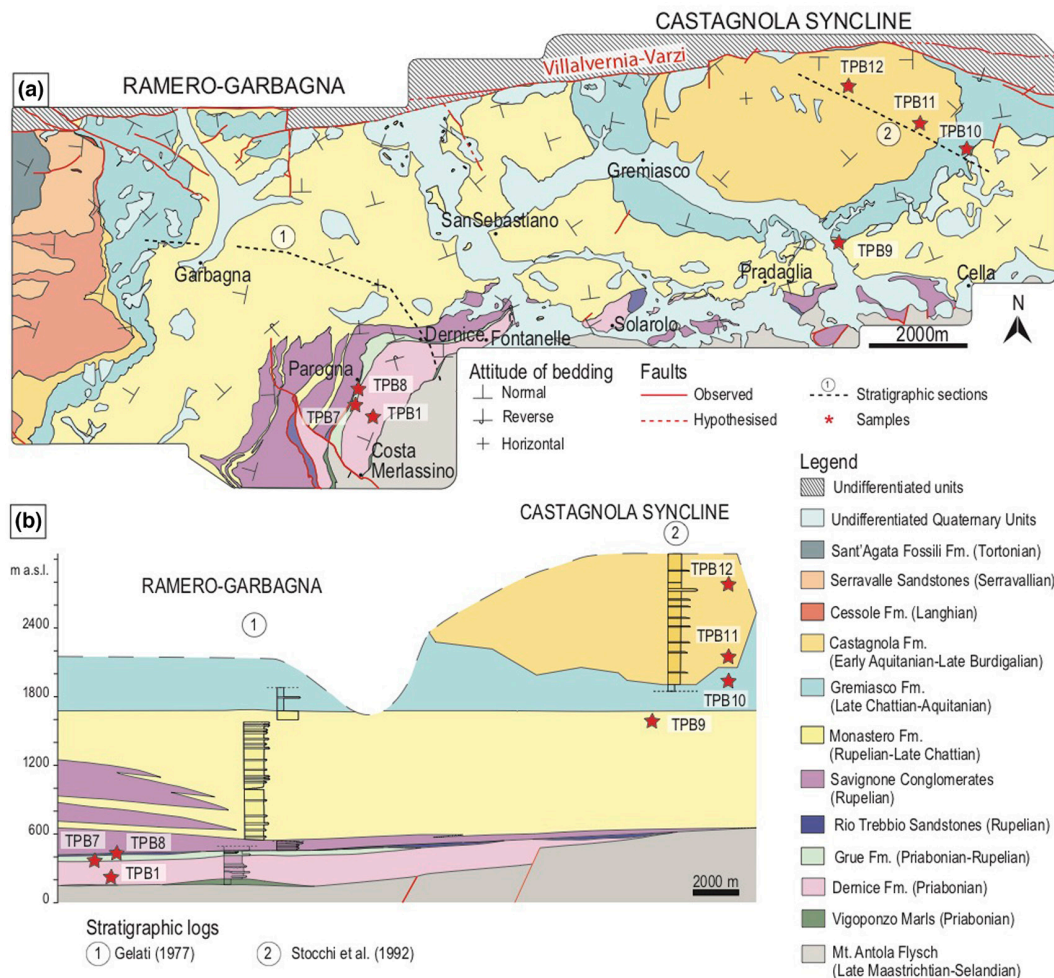
FIGURE 3 Geological map of the study area. (a) the Borbera-Curone deponcentre in the eastern TPB; see Figure 1c for location (lithostratigraphy after Gelati, 1977; Cavanna et al., 1989; Marroni, Meneghini, & Pandolfi, 2010, Marroni, Ottria, & Pandolfi, 2010; Festa et al., 2015), with location of sampling sites. (b) lithostratigraphic cross-section flattened at the Gramiasco-Monastero Formation boundary with stratigraphic location of samples.

covers the metamorphic basement of the Ligurian Alps. The succession starts with coarse-grained/pebbly units of the Molare Fm. of early Oligocene age (34–28.4 Ma; Gnaccolini et al., 1998) overlain by upper Oligocene to Tortonian hemipelagic mudstones and deep-water turbidites.

2.3 | Previous geo-thermochronometric dataset and current geothermal gradient

Heat flows continuously from the interior of the earth towards the surface and supplies the bulk of energy that heats buried sediments. However, high heat flow is unevenly distributed, able to trigger mantle upwelling where the lithosphere is thinned, in tectonically active regions (enhanced by rapid exhumation of deep hot crustal blocks) or where volcanism occurs. In summary, spatial and temporal lithospheric inhomogeneities account for

the uneven flow of heat through rocks, generating geothermal anomalies. Due to such inhomogeneities, each region must be considered separately when collecting tectono-stratigraphic observations, thermal indicator data (among others, AFT and fluid inclusions), and eventually constructing numerical models. The TPB and its margin have been the object of several geochronological and thermochronometric investigations, resulting in a complex dataset including high- to low-temperature chronometers (Figure 4). A complete presentation of the dataset is provided in the Supporting Information (Table S1). The main thermal signals in the study area are as follows:

1. A late Eocene–early Oligocene stage characterized by relatively rapid cooling (from about 400°C to surface conditions) of the metamorphic basement of the Ligurian Alps, recorded by $^{40}Ar/^{39}Ar$, zircon fission-track (ZFT) and zircon U-Th/He (ZHe) ages that are similar to—or even younger than—the adjacent TPB

basal deposits of the Molare Fm. There is a general agreement in interpreting this cooling stage as the result of rapid syn-compressional exhumation of Ligurian Alps basement rocks (Barbieri et al., 2003; Carrapa et al., 2004; Federico et al., 2005; Maino et al., 2012, 2013; Vignaroli et al., 2008, 2010).

2. A Chattian-Aquitanian cooling event recorded by AFT, detrital mica ^{40}Ar/^{39}Ar and apatite (U-Th)/He (AHe) ages from both the metamorphic rocks of Ligurian Alps (Briançonnais and Voltri massifs) and the basal clastic deposits of TPB (Molare Fm.). This thermal signal has been interpreted to represent exhumation of the Western Alps (Carrapa et al., 2016), and coeval postdepositional heating and subsequent cooling related to early Oligocene subsidence followed by late Oligocene northward depocentre migration and tectonic uplift (Bertotti et al., 2006).

Presently, temperatures up to 70–80°C have been measured at multiple hot-spring localities in the Alps and TPB (e.g. Acqui Terme, see Figure 1 for location), and have been interpreted as associated with localized, transient thermal anomalies rather than a regional signature (Luijendik et al., 2020; Pasquale et al., 2011; Spooner

et al., 2020). In the case of the TPB, this means that the groundwater heats up when in contact with (or flowing through) the metamorphic basement of the Ligurian Alps (Pasquale et al., 2011). However, the geothermal gradient has been calculated only in wells located close to the Po Plain foredeep basin, which has undergone a severe subsidence phase and consequent filling of marine clastic sediments since the Late Miocene (ca. 6–7 km maximum thickness, Pieri & Groppi, 1981; Amadori et al., 2018, 2019). The same magnitude of subsidence did not occur in the episutural TPB, which does not have (and never experienced) a similar thick cold Plio-Quaternary sedimentary cover able to buffer the regional heat flow.

Given the lack of thick succession in the TPB to buffer regional heat flow, this paper demonstrates that there was a regional thermal anomaly influenced by mantle upwelling that heated the basin, along with its metamorphic basement, between 35 and 30 Ma.

3 | MATERIALS AND METHODS

We apply a multi-method analytical approach to characterize the temporal and stratigraphic relationships
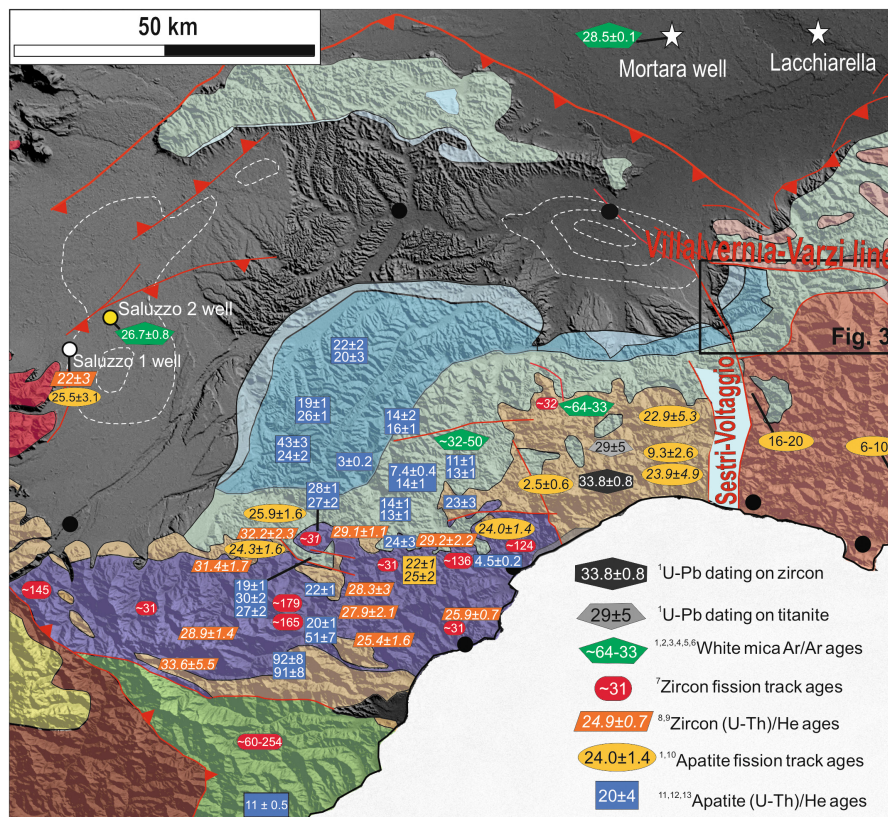
FIGURE 4 Geo-thermochronometric dataset compilation. All new and literature data (Table S1) are plotted on a synthetic tectonic map of the Ligurian Alps and Tertiary-Piedmont Basin. For legend of geology and symbols, refer to Figure 1. [1]Vignaroli et al. (2010); [2]Federico et al. (2005); [3]Barbieri et al. (2003); [4]Carrapa et al. (2003); [5]Carrapa et al. (2004); [6]Carrapa et al. (2016); [7]Vance (1999); [8]Decarlis et al. (2017); [9]Maino et al. (2012); [10]Balestrieri et al. (1996); [11]Foeken et al. (2003); [12]Mosca (2006); [13]Bertotti et al. (2006).

between deposition and basin thermal history of the entire sequence of the eastern TPB. Herein, we briefly summarize the samples and applied methodologies, which are described in full in the Supporting Information text and tables.

3.1 | Low-temperature thermochronology

Apatite fission-track analysis (AFT), by means of the external-detector method (e.g. Donelick et al., 2005; Green, Duddy, Gleadow, & Lovering, 1989; Green, Duddy, Laslett, et al., 1989; Hurford & Green, 1983), was completed on all seven detrital samples (Table 1). Sample preparation and data acquisition were performed at the University of Arizona Fission Track Laboratory following the standardized procedures and protocols described in Donelick et al. (2005) and Kohn et al. (2019). The standard glass CN-5 was used as a dosimeter to measure the neutron fluence during irradiation at the Oregon State TRIGA Reactor, Corvallis (Oregon, USA) with a nominal neutron fluence of 1.2×10^{16} n/cm^2. Apatite fission-track ages ($\pm 1\sigma$, Galbraith & Laslett, 1993) were calculated using the zeta-calibration method with a zeta factor of 342.2 ± 11 (C.A. analyst; Hurford, 1990; Hurford & Green, 1983) estimated using IUGS standards (Durango and Fish Canyon apatite crystals) and a value of 0.5 as geometry correction factor. Single-grain age distributions were decomposed into components (i.e. age populations) using radial plotter by Vermeesch (2012). To constrain the cooling history through the apatite partial annealing zone, horizontal confined track lengths were measured for samples TPB1 and TPB7.

Apatite (U-Th-Sm)/He dating (AHe) was performed on the two lowest samples TPB1 and TPB7 in order to evaluate the degree of heating at the bottom of the sequence. Analyses were completed at the Radiogenic Helium Dating Laboratory of the University of Arizona, using the methodology described in Reiners et al. (2004). Ten apatite crystals (five grains from sample TPB1 and from TPB7) were dated. Euhedral or sub-euhedral inclusion-free apatite crystals with widths >60 μm were chosen for analysis as recommended by Ehlers and Farley (2003). Single crystals were loaded in 0.8 mm-thick Nb tubes and then degassed under vacuum by heating using Nd-YAG laser. Concentrations of ^{4}He were measured by ^{3}He isotope dilution and measurement of the ^{4}He/^{3}He ratio through a quadrupole mass spectrometer. The degassed apatite crystals (and the tube) were then dissolved in nitric acid and the concentrations of U, Th, and Sm were measured using an inductively coupled plasma mass spectrometer (ICP-MS). Alpha ejection correction was applied to the calculated AHe ages, taking into account the dimensions of the crystal (Ketcham et al., 2011).

3.2 | Inverse thermal modelling

Inverse thermal history modelling of thermochronological data was performed using QTQt 5.8.0 package (Gallagher, 2012), in order to extract the most probable thermal history for the observed data and associated uncertainty. The QTQt software applies a Bayesian approach to inverse thermal history modelling by using the reversible jump Markov chain Monte Carlo (MCMC) method, described in detail in Gallagher et al. (2005) and Gallagher (2012). The theoretical basis and application of

TABLE 1 Information on samples and analyses performed

Sample name	Latitude	Longitude	Lithostratigraphy		Stratigraphic age	FIM	AFT (*lengths)	AHe
TPB1	N44° 45.239′	E9° 02.358′	Dernice Fm.		Late Pribonian-Earliest Rupelian	x	x*	x
TPB7	N44° 45.313′	E9° 02.028′	Grue Fm.		Earliest Rupelian	x	x*	x
TPB8	N44° 45.434′	E9° 02.040′	Rio Trebbio Fm.		Early Rupelian	x	x	
TPB9	N44° 46.969′	E9° 08.994′	Monastero Fm.		Late Rupelian	x	x	
TPB10	N44° 47.943′	E9° 10.741′	Gremiasco Fm.	Nivione Mb.	Chattian	x	x	
TPB11	N44° 48.214′	E9° 10.286′	Castagnola Fm.	Lower Costa Grande Mb.	Early Aquitanian	x	x	
TPB12	N44° 48.603′	E9° 09.348′		Lower Arenaceo Mb.	Late Aquitanian-Earliest Burdigalian	x	x	

Note: See also Figure 3 for sample locations on map.

Abbreviations: AFT, apatite fission track analysis; AHe, apatite (U-Th-Sm)/He dating; FIM, fluid inclusion microthermometry.

Basin Research | IAS EAGE—WILEY | 9

TABLE 2 Results of apatite fission track analysis

Sample	Formation	Stratigraphic age (Ma)	No. of grains	Spontaneous ρs (10^5 tr/cm^{-2})	Ns	Induced ρi (10^5 tr/cm^{-2})	Ni	Dosimeter ρd (10^5 tr/cm^{-2})	Nd	Central age ±1σ (Ma)	P(χ²)	Disp. (%)	Population 1 Age ±1σ (Ma)	Population 2 Age ±1σ (Ma)	Dpar Mean ±1σ (µm)	Measured Length Mean track length ±1σ (µm)	Stand. Dev	No. of lengths	c axis correction Mean track length ±SD (µm)
TPB1	Dermice	35.5–33.5	109	3.73	853	33.33	7623	13.03	2612	24.8±1.3	0.01	18	24.9±1.2		1.67±0.15	12.4±0.13	1.3	100	13.6±1.2
TPB7	Grue	33.75–32.5	100	3.8	704	24.51	4555	13.76	2716	41.9±3.2	0	48	31.8±2.3	78±12	1.83±0.24	12.6±0.19	1.4	54	13.9±1.06
TPB8	Rio Trebbio	32.5–32	53	4.38	261	29.66	1765	14.29	2831	35.4±3.4	0	35	36.1±2.7		1.69±0.16				
TPB9	Monastero	30–28.5	105	6.34	1695	43.1	11,505	14.95	2954	37.4±1.8	0	21	33.6±2	50.6±5	1.84±0.38				
TPB10	Nivione	27.5–24.5	104	3.84	1073	29.11	8128	15.4	3039	36±2.2	0	37	28.9±1.6	68.7±7.2	1.79±0.19				
TPB11	Castagnola	22.25–22	66	7.42	1153	31.87	4947	14.18	2800	55.5±4.1	0	42	41.9±2.7	88.2±6.5	1.74±0.28				
TPB12	Castagnola	21.6–16	60	2.49	333	22.54	3009	13.24	2614	25.6±2	0.01	25	25±1.7		1.64±0.18				

Note: Central ages calculated using dosimeter glass CN5 and $\xi = 342.23 \pm 11.17$ (C.A. analyst). ρs: spontaneous track densities measured in internal mineral surfaces; Ns: total number of spontaneous tracks; ρi and ρd: induced and dosimeter track densities on external mica detectors; Ni: total numbers of induced tracks; Nd: total numbers of tracks in dosimeter. $P(\chi)^2$: probability of obtaining χ^2-value for ν degrees of freedom (where ν = number of crystals−1); a probability >5% is indicative of a homogeneous population. RadialPlotter automatically performs a χ^2-test for statistical homogeneity of fission track data. For populations that have failed this test, RadialPlotter program implements the mixture modelling algorithm of Galbraith and Green (1990). Stratigraphic ages: TPB1: Mancin and Pirini (2001); TPB7-TPB8: Marroni, Meneghini, and Pandolfi (2010); Marroni, Ottria, and Pandolfi (2010); TPB9: Gelati (1977); TPB10: Mancin and Pirini (2001); TPB11-TPB12: Andreoni et al. (1981), Marini et al. (2020).

this modelling technique have been well documented and discussed in several case studies, among others Wildman et al. (2017).

Apatite fission-track single-grain ages, confined track length distributions and AHe ages were modelled along with geological constraints, the formation depositional ages and the present-day surface temperature of $15 \pm 5°C$. The kinetic parameter used is the D_{par} (Donelick, 1993), which represents the c-axis parallel etch pit size predominantly influenced by the relative proportions of Cl and F (Carlson et al., 1999; Sobel & Seward, 2010). The multi-kinetic annealing equation from Ketcham et al. (2007) and c axis projection (to correct length measurements) from Ketcham (2005) was used. The minimum number of burn-in and post burn-in iterations is 10^5.

We modelled the thermal history of the two lowermost samples which yielded AFT ages younger than the depositional age: samples TPB1 and TPB7 (Tables 2 and 3). All concordant AHe single-grain ages yielded by sample TPB1 were jointly inverted alongside their corresponding AFT data by using the radiation damage accumulation and annealing model of Gautheron et al. (2009).

3.3 | Fluid inclusion microthermometry

Fluid inclusion microthermometry (FIM) was performed on pore space filling diagenetic minerals from seven sandstone samples to better constrain the thermal history experienced by the rocks and circulating fluids (Goldstein, 2001). Prior to microthermometric measurements, petrographic observations were made to distinguish the primary fluid inclusions trapped during mineral growth (Goldstein, 2001; Goldstein & Reynolds, 1994). Analyses were performed at the University of Pavia using a Linkam THMSG 600 heating-freezing stage, mounted on an Olympus BX51 microscope. Low heating rates were used for measuring homogenization temperatures (Th) to avoid overheating. The accuracy of the microthermometry data is ±1°C.

3.4 | Assessment of stratigraphy depth and burial

Seven samples (see Table 1 and Figure 4 for locations) of medium-grained clastic sedimentary rocks were collected along previously investigated sections (Di Giulio, 1991; Marini et al., 2016). Each lithostratigraphic unit is assigned an age constrained by biostratigraphy and/or magnetostratigraphy, spanning from Priabonian to earliest Burdigalian, and a thickness (Di Giulio, 1991; Gelati, 1977; Mancin & Pirini, 2001; Marini et al., 2020). To track the

TABLE 3 Results of AHe analysis

	He (pmol)	Th/U	Correction factors Ft ^{238}U	Ft ^{235}U	Ft ^{232}Th	Ft ^{147}Sm	Rs (um)	U (ppm)	Th (ppm)	Sm (ppm)	^{4}He (nmol/g)	Mass Ap (g)	eU* (ppm)	Raw age ±1σ (Ma)	Fully corrected age (Ma) Ft Corr. age (Ma)	±1σ (Ma)
TPB1	0.00113	1.44	0.630	0.582	0.582	0.878	37.14	19.1	26.7	201.0	1.79	6.3008E−07	25.36	12.94 ±0.26	20.90	0.43
	0.00236	1.51	0.589	0.538	0.538	0.864	32.97	39.5	58.0	333.7	3.40	6.9531E−07	53.12	11.75 ±0.18	20.37	0.32
	0.00306	2.40	0.678	0.635	0.635	0.895	43.39	28.9	67.4	616.3	3.11	9.8352E−07	44.73	12.65 ±0.19	19.01	0.28
	0.01164	0.52	0.672	0.629	0.629	0.893	42.58	60.7	31.0	254.5	8.67	1.3430E−06	68.03	23.48 ±0.32	35.17	0.48
	0.00409	1.63	0.620	0.571	0.571	0.875	36.00	28.9	45.9	482.2	6.48	6.3054E−07	39.64	29.77 ±0.43	48.84	0.71
TPB7	0.01327	17.34	0.811	0.784	0.784	0.940	59.84	7.6	128.8	309.2	3.99	3.3291E−06	37.89	19.16 ±0.26	24.23	0.31
	0.04640	2.14	0.813	0.787	0.787	0.940	57.56	29.2	60.8	249.6	6.90	6.7235E−06	43.45	29.12 ±0.31	38.80	0.40
	0.02246	1.54	0.813	0.787	0.787	0.940	61.09	24.4	36.6	231.5	5.10	4.4013E−06	32.96	28.37 ±0.32	35.16	0.40
	0.01724	0.15	0.798	0.770	0.770	0.936	63.90	31.0	4.6	151.2	3.93	4.3873E−06	32.11	22.55 ±0.31	28.28	0.39
	0.00260	26.29	0.687	0.646	0.646	0.899	46.05	10.1	258.8	130.7	3.09	8.4129E−07	70.90	7.99 ±0.13	12.25	0.20

Note: eU* (effective uranium) is calculated as eU ppm = (U ppm) + (0.235 [Th ppm]). Rs is the radius of a hypothetical sphere that should approximate the crystal. It is calculated as the mean between the two dimensions measured in each single grain. Raw age (±σ): age of the grain before the correction. Correction factors (Ft) after Ketcham et al. (2011), assuming homogeneous distribution U and Th. Fully corrected AHe age = Raw AHe age/Ft. Estimated uncertainty is equal to 1σ analytical uncertainty, which includes error propagated from U, Th, Sm, and He measurement uncertainties.

progression of sample's burial depth with time, the decompacted thickness of the basin sequence was calculated following Van Hinte (1978). Data used for calculation of decompacted thickness are shown in Table S2 and described in the supplemental materials.

3.5 | 2-D thermal numerical modelling

The TPB experienced a complex interplay of tectonic process since its formation as it developed on an exhumed orogen and was subsequently affected by stretching of the lithosphere related to the opening of the Liguro-Provençal rift basin. Oligocene–Miocene magmatism has also been documented in the TPB sedimentary sequences (e.g. Di Giulio et al., 2001). Such complexity is here tested through three end-member models for generating thermal anomalies in the shallow crust: (i) advection due to fast exhumation of deep basement rock units, (ii) mantle upwelling and (iii) advection of melts during magmatic underplating due to lithospheric stretching. This modelling approach aims to quantify the relative contribution of each

end-member mechanism to the overall thermal budget. A purely thermal version of the finite differences code evp2d (Casini, 2012; Casini et al., 2013; Casini & Maino, 2018; Maino et al., 2020; Secchi et al., 2022) was used to run a suite of 2-D numerical experiments devised to evaluate different heating scenarios. Governing equations are provided in the supplemental material.

The model set-up was designed to simulate a 500×200 km section oriented roughly NNE–SSW across the Alps-northern Apennines transition zone, where the basin overlies an Alpine orogenic wedge composed of low-grade metamorphic rocks and sedimentary cover (Figure 5a). The geometry and thickness of the various layers have been defined based on the high-resolution tomography according to Lippitsch et al. (2003), Ziegler and Dèzes (2006), Di Stefano et al. (2011), Kästle et al. (2020) and Handy et al. (2021). The composition and physical properties of the different materials used to simulate the basin fill and the orogenic wedge, together with the subcontinental mantle and the European and Adria plates, are detailed in the Supporting Information (Table S5). The experimental domain is discretized through conservative
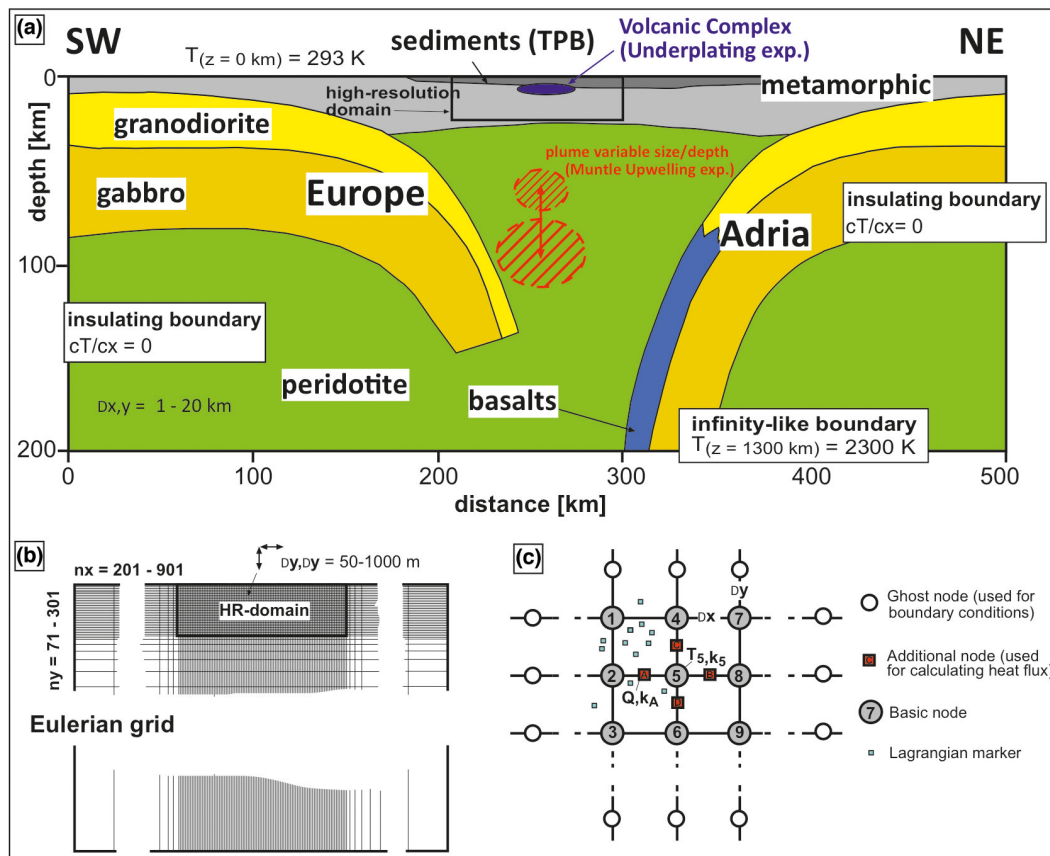
FIGURE 5 Thermal Model setup. (a) 2-D transect showing the three tested heating processes (i.e. fast exhumation of hot rock units, asthenospheric plume and advection of melts) with spatial and thermal boundary conditions. (b) Experimental domain discretized through finite Eulerian grid. (c) Basic and additional flux nodes of the Eulerian grid. See text and Supplementary Information for full details of material properties and thickness of the various layers.

finite differences using an Eulerian grid composed of basic nodes and additional flux nodes that allow lateral variation of thermal conductivity (Vosteen & Schellschmidt, 2003) (Figure 5b,c). The grid provides a maximum cell resolution of 1 ×1 km in a central-upper 100 by 30 km domain coincident with the TPB. Only the experiments simulating magmatic underplating use a finer grid that ensure a high spatial resolution (50 ×50 m cell size) in the central domain, allowing them to portray the thermal structure of the contact metamorphic aureole around the magmatic body.

The first set of experiments explores the thermal signal recorded at the base of TPB in response to exhumation from 3.5 km depth, which represents the maximum decompacted thickness of the basin. The full spectrum of exhumation rate variability (between 2 to 40 mm/yr; see Maino et al., 2012; Fox et al., 2015, 2016) and thicknesses of the orogenic wedge underlying the basin (15–25 km) have been considered. The second set of experiments addresses the effect of mantle upwelling (i.e. asthenospheric plume) resulting from rollback and/or break-off mechanisms. Due to the purely thermal nature of the experiments, no attempt was made to discriminate between slab rollback and break-off, as the two mechanisms likely produce similar heating signals in the shallow crust. Mantle upwelling is simulated by producing different subcrustal thermal anomalies of variable radius (30–60 km) and depth beneath the surface (60–90 km). The ranges of size and location of heat sources are constrained based on interpretation of the lithospheric disjunction imaged by deep seismic tomography at the Alps-Apennines transition zone (Handy et al., 2021; Kästle et al., 2020; Piromallo & Faccenna, 2004; Sinclair, 1997; von Blanckenburg & Davies, 1995).

A third set of experiments evaluates the effect of magmatic underplating (Whittington et al., 2009) under different conditions such as variable thickness of the magmatic body, connectivity between different magmatic channels and different magma injection rates from about 4 to 57 mm/yr. In this set of experiments, the emplacement depth and thickness of a tabular magmatic body are derived from geophysical constraints and borehole data (Fantoni et al., 1999; Mattioli et al., 2002). Magma injection rates are simply expressed as time-averaged vertical growth rates of the volcanic complex (Annen et al., 2006; Annen, 2011). Finally, the combined effect of exhumation and mantle upwelling is also investigated using different vertical velocities and depths of the rising asthenosphere (2–8 mm/yr). The last three sets of experiments use an initial geothermal gradient of 25°C/km which is consistent with the surface heat flow data and borehole measurements (Pasquale et al., 2012; Pauselli et al., 2019). Only the first set of experiments simulating the effect of variable

exhumation rates assumes a higher initial geothermal gradient of 35°C/km to ensure that the base of TPB reaches the temperature recorded by sample TP1 at the onset of the simulation.
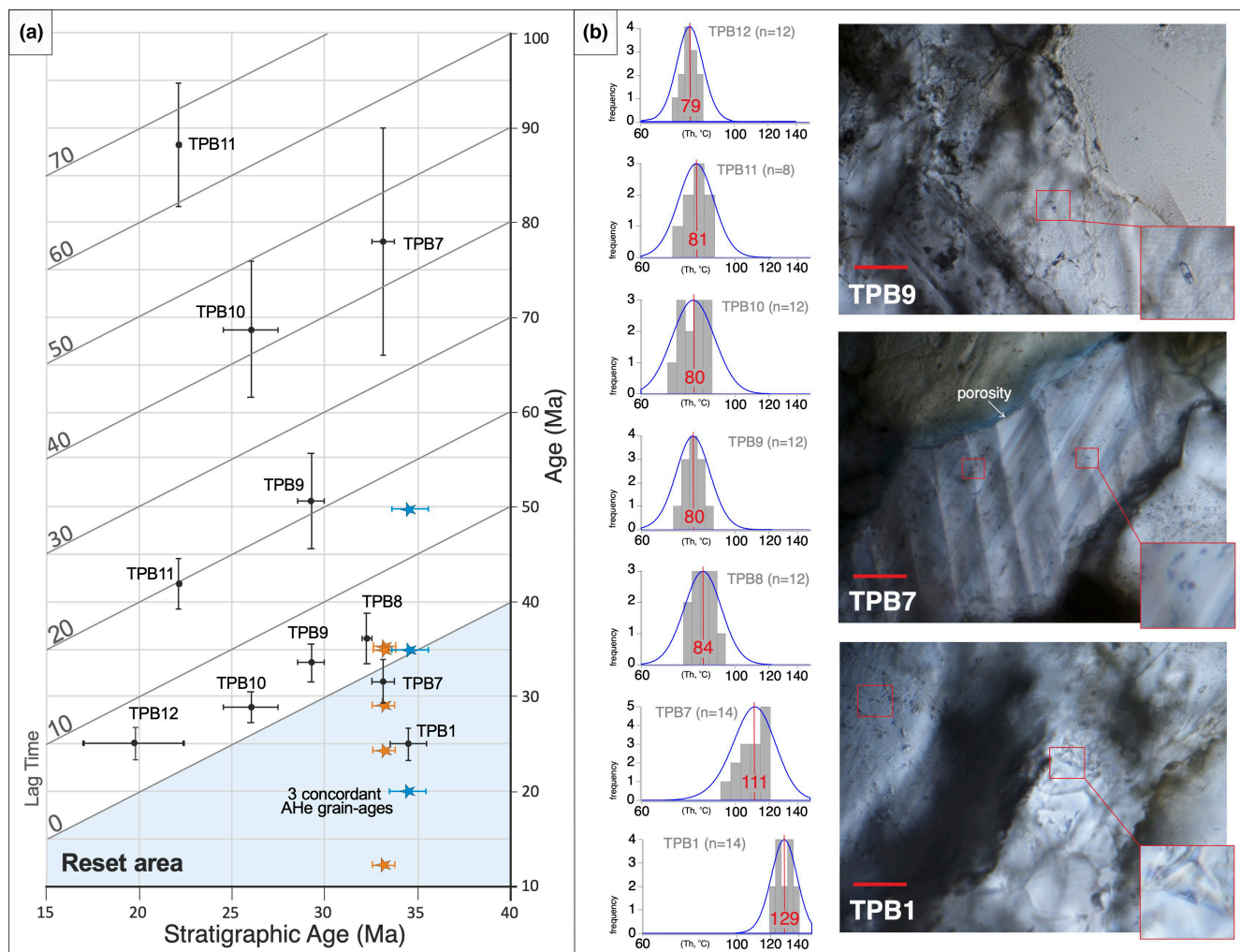
4 | RESULTS

4.1 | AFT and AHe dating

The results of the low-T thermochronometric investigations are shown in Figure 6a, Tables 2 and 3 (see also Figures S1A and S2 and Table S4 in the Supporting information). For the AFT determinations, between 53 and 109 grains were dated per sample, with central AFT ages in the range of ca. 25 to 56 Ma. Measurements of D_{par} were made for each sample as a proxy for the chemical compositional influence (Cl and F content) on track annealing, and range from 1.4 to 2.24 μm.

The stratigraphically lowest (Priabonian) sample TPB1 is the only one showing a single post-depositional peak age at 24.9 ±1.2 Ma ($n = 109$, six grains with zero spontaneous tracks) and mean track length distribution of 12.4 ±0.13 μm ($n = 100$, ± standard deviation), corrected for c axis projection 13.6 ±1.2 μm (± standard deviation). Sample TPB7 from the overlying formation (deposited between 33.75 and 32.5 Ma, Rupelian) contains two age populations, the younger of which is as old as (within the error) the depositional age. In this sample, 54 horizontal confined tracks lengths were measured, with a mean track length of 12.6 ±0.19 μm (corrected for their c axis orientation in 13.9 ±1.06 μm, ± standard deviation) (see Table S4 in the supplemental material). Measuring the angle between horizontal track lengths and the c axis of the analysed grain accounts for anisotropic annealing and etching of tracks. The influence these effects have on the fission-track age and length data is considered during thermal history modelling. Track length distributions are unimodal and negatively skewed for sample TPB1 and unimodal for sample TPB7.

Up succession, all samples yield AFT ages older than the depositional ages. Three samples (TPB1, TPB8 and TPB12) contain only one AFT population age, whereas the other four samples (TPB7, TPB9, TPB10 and TPB11) contain two age populations. Population 1 comprises ages in the range of 28.9 ±1.6 to 41.9 ±2.7 Ma. It is also the most abundant, encompassing 68%–79% of the sample grain aliquot. Ages clustered in population 1 and the single population ages from TPB1, TPB8 and TPB12 plot on a quasi-constant isolag-time line (ca. 5 Myr), getting younger up-section (Figure 6a). Population 2 clusters between 50.6 ±5 and 88.2 ±6.5 Ma and is always older than population 1 and the respective stratigraphic age. This

FIGURE 6 Results of low-T thermochronometry and microthermometry analyses. (a) detrital apatite fission-track population ages and AHe ages versus depositional age of the stratigraphic unit. Light blue indicates the area where AFT (black circles) and AHe ages (blue stars: TPB1; orange stars: TPB7) are younger than stratigraphic ages. AFT ages are also shown in radial plots in Figure S1 in the Supplemental Material. AHe age error is expressed within the shape of the symbol because is <1 Ma. Diagonal lines represent iso-lag times every 10 million years (Figure 6a). (b) left column: frequency histogram of homogenization temperatures (Th) in calcite cements (see Table S4 in the Supplemental Material). Red line corresponds to the median Th value. Blue line: Kernel Density Estimation. Right column: examples of cements and fluid inclusions from thick sections image. Red bar is 25 μm scale. Porosity is evidenced by blue epoxy impregnation.

second population (which comprises ca. 20%–30% of the sample grains) results in a variable lag time from ca. 15 to 70 Myr, and it does not align on a single isolag-time line (Figure 6a).

Regarding AHe dating, three of five crystals from sample TPB1 yield reproducible ages, in the range of 19 ± 0.3 and 20.9 ± 0.4 Ma, with a standard deviation <20% of the mean age. These ages are all younger than both the AFT and depositional age of the same sample. The remainder of grains yielded ages older than their respective stratigraphic ages, 35.17 ± 0.48 and 48.84 ± 0.71 Ma. Apatite grains from sample TPB1 show neither AHe age-grain size (i.e. the grain spherical equivalent radius) nor age-eU concentration correlations (Figure S2A in the supplemental material). All single grain AHe ages from sample

TPB7 are not reproducible within the analytical uncertainties, yielding a range of ages between ca. 12 and 36 Ma (Table 3). Three out of five crystals yield ages younger than the AFT and respective stratigraphic age (12.25 ± 0.2 Ma, 28.3 ± 0.4 Ma and 24.2 ± 0.3 Ma). In contrast to sample TPB1, sample TPB7 shows a correlation ($R^2 = 0.62$) between AHe age and eU concentration (Figure S2B in the supplemental material).

4.2 | Thermal inverse modelling

The confined track length distribution, corrected for *c* axis horizontal projection according to Ketcham (2005), from samples TPB1 and TBP7 were used to reconstruct the

thermal history of the basin (Table S3 in the Supplemental Material). For confined track lengths to be useful in producing thermal histories, the original length of newly formed tracks must be constrained. We considered unannealed, induced tracks in Durango apatite with the mean track length of 16.3 μm after Gleadow et al. (1986). For each model, 10^5 burn-in and post-burn-in models were used with a thinning factor of 1, meaning that all post-burn in were used.

Inverse thermal history modelling of sample TPB1 utilizes AFT central ages, single-grain age distribution, confined track length distribution and AHe ages from the same sample (see Figure 7a where geological constrains are also shown).

The QTQt expected model for the basal sample (Figure 7a) indicates that the Priabonian–Rupelian succession experienced high temperatures rapidly after deposition: ca. 120°C between 35 and 30 Ma, before cooling through PAZ window between 30 and ca. 20 Ma with 6–7°C/Myr cooling rate. Finally, a slow cooling rate is observed <20 Ma from 40°C to present-day surface temperature (15 ± 5°C) at 1–2°C/Myr.

The QTQt expected model for sample TPB7 (Figure 7b) describes a post-depositional heating of a lower magnitude than the lower TPB1 sample. The resolved thermal history model shows fast-heating to a peak temperature of ca. 90°C at ca. 35–30 Ma, followed by slow, monotonic cooling (ca. 2°C/Myr) up to present-day surface conditions. In this case, AHe ages were not included in the model because no single-grain ages are replicable (Table 3).

4.3 | Fluid inclusion microthermometry

Table 4 and Figure 6b summarize the microthermometric results for the studied fluid inclusions in authigenic
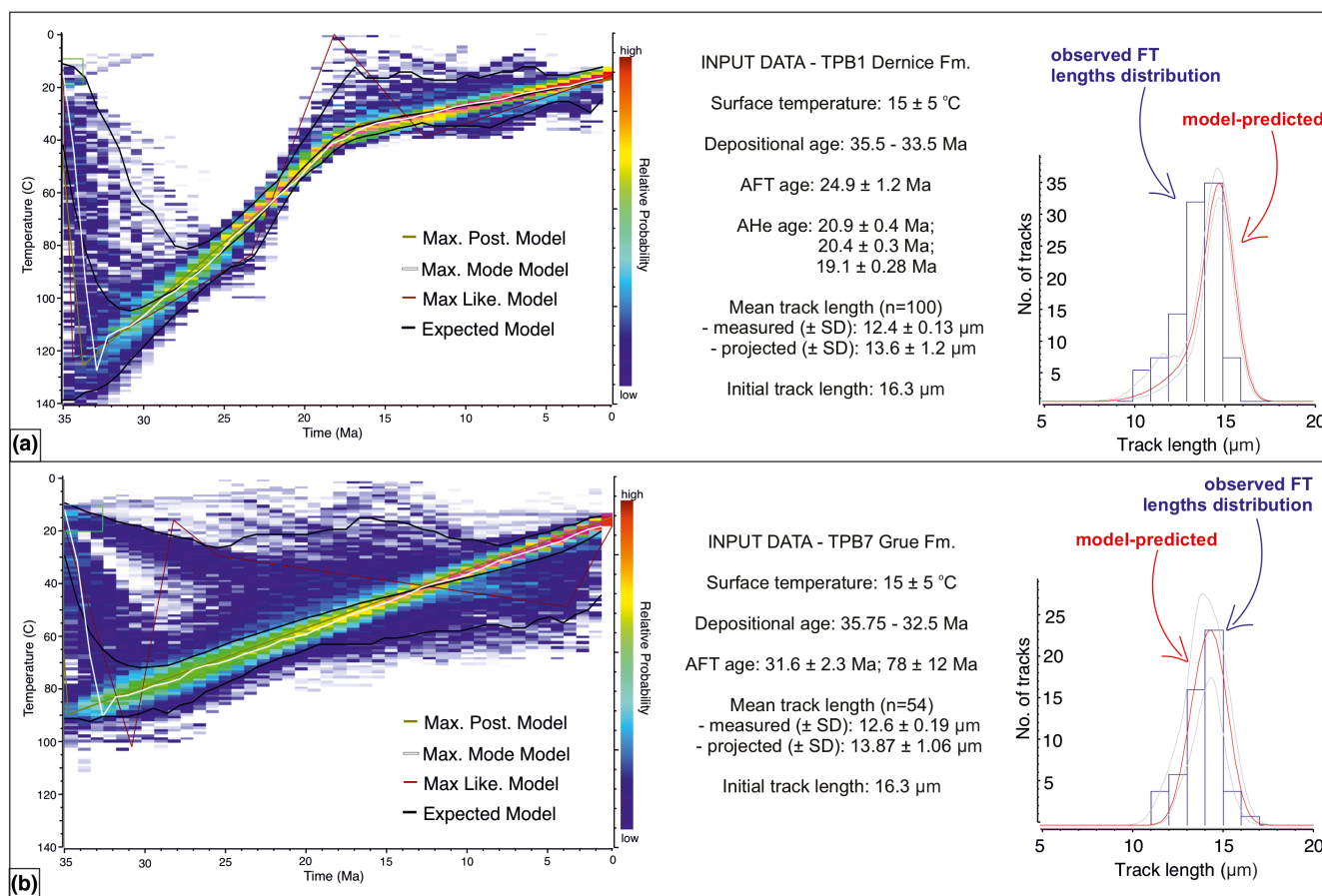

FIGURE 7 Inverse thermal models of basal samples from Borbera-Curone sub-basin. (a) Expected Time–temperature model of TPB1 (left) and comparison between observed (and projected) and model-predicted length measurements (right). (b) Expected Time–temperature model of sample TPB7 (left) and comparison between observed (and projected) and model-predicted length measurements (right). All models were performed using QTQt (Gallagher, 2012). Max Likelihood Model: t–T history that best fit the input data, although of the overcomplex. Max Posterior Model: simpler than Max Likelihood because includes fewer t–T paths. Max Model: obtained from the distribution of all models sampled. Expected Model is effectively a weighted mean model, where the weighting is provided by the posterior probability for each model. See also the software user guide for more details.

TABLE 4 Results of fluid inclusions microthermometry

Sample	Formation	Inclusion phase	Cement	No. inclusions	Th (°C) Range	1 Std dev.	Median
TPB1	Dernice	L + V	Calcite	14	120–137	5.39	129.0
TPB7	Grue	L + V	Calcite	14	99–118	7.53	110.5
TPB8	Rio Trebbio	L + V	Calcite	12	76–90	5.01	84.0
TPB9	Monastero	L + V	Calcite	12	72–86	4.23	79.5
TPB10	Nivione	L + V	Calcite	12	72–88	5.65	79.5
TPB11	Castagnola	L + V	Calcite	8	74–88	4.61	81.0
TPB12	Castagnola	L + V	Calcite	12	72–85	3.89	78.5

Note: Average values for the different measurements are shown along with standard deviation (complete dataset shown in Table S4, Supplementary material). Th: temperature of homogenization. L + V: bi-phase fluid inclusion with liquid + vapour. No. is the number of inclusions measured per sample.

calcite (see also Table S4 in the supplemental material). They occur mostly as pore-filling cement (estimated average of 13.7% of the solid rock), and subordinately as patches extending from the pore-space to framework grains (3.5% of the solid rock as an average). Notably, authigenic calcite constitutes the cement of all samples with compaction-dominated diagenesis and chlorite cement is rarely observed.

Calcite cements are characterized by bi-phase liquid-rich fluid inclusions (FIs), containing a vapour bubble and a colourless liquid, that are useful for Th measurements. The bi-phase FIs occur isolated or in patches with consistent sizes (3–10 μm) but in variable shape, perhaps controlled by crystallographic planes. All the observed FIs (mono- and bi-phase) contain an aqueous fluid and no hydrocarbon phase, as suggested by the lack of fluorescence when observed under UV-light. Eighty-four bi-phase inclusions were considered for microthermometry analyses. Complete homogenization occurred in the liquid phase for all inclusions.

All samples present a single Th peak. Fluid inclusions in calcite cement from the lowest samples TPB1 and TPB7 describe a crystallization environment characterized by temperature homogenizing between ca. 100 and 140°C. Conversely, all shallower samples from TPB8-12 experience homogenization temperatures in a range of 70–90°C.

4.4 | Burial history

The sample TPB1, from the lowermost stratigraphic unit, Dernice Fm. (35.5–33.5 Ma, Gelati, 1977) yields an AFT age of 25 Ma, which is younger than the depositional age of the hosting strata. This sample was buried by sediments with a decompacted thickness of ca. 2.3 ±0.1 km until ca. 25 Ma (Figure 8) and was later cooled as shown in Figure 7. When considering the present-day geothermal gradient of the western Po Plain of 26°C/km (Pasquale et al., 2012),

and a surface temperature of 15 ± 5°C, the expected temperature at a depth of 2.3 ±0.1 km falls in the range of 66–82°C (Figure 8). These temperatures are within the AFT partial annealing zone (PAZ; ca. 120–60°C; Ehlers & Farley, 2003), and therefore not enough to completely anneal the tracks formed during the pre-burial history of the sample. To reset the AFT age at this depth, a palaeogeothermal gradient of 45 ± 5°C/km is required (Figure 8). The sample stratigraphically above (TPB7) was buried by ca. 1.7 km of sediments; here, AFT populations yield both reset and non-reset ages, possibly as the result of residence at temperatures within the PAZ.

4.5 | 2-D thermal numerical modelling

The 2-D thermal numerical experiments were devised to test different geological process (i.e. exhumation of rocks with relatively high-temperature fields, mantle upwelling or magmatic underplating) to explain the high temperatures of ca. 100 ± 10°C recorded at the base of TPB, which cannot be explained by the reconstructed burial depth of 2.3 km (Section 4.5). The results from the thermal model (Sections 4.5.1–4.5.4) show how thermal anomalies may differ in spatial extent (laterally and vertically), intensity and duration. However, all these characteristics can be resolved by constraining time–temperature paths of the rocks affected by the thermal anomaly, producing insights into the geological processes that are responsible for the anomaly (Figure 9 and Table 5).

4.5.1 | Variable exhumation rates

In the first set of experiments, the thermal structure of the shallow crust was constrained for exhumation rates varying from 2 to 40 mm/yr. The model does not consider the exhumation kinematics; thus, it indifferently accounts for
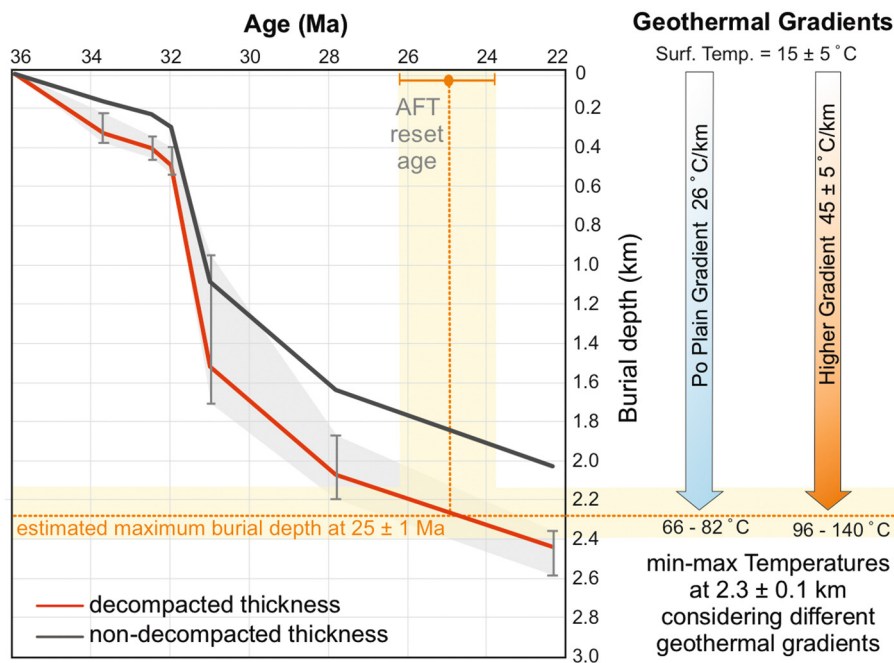
FIGURE 8 Burial history diagram and palaeo-geothermal gradient estimations. Depth-time path of sample TPB1, corrected for compaction with the equation of Van Hinte (1978). The red line images the decompacted thickness calibrated using best estimates of compaction coefficients derived by direct measurements of lithological fractions. Error bars (in grey) acknowledge the uncertainty in precisely established lithological fractions (Table S1). Back line shows the cumulative lithostratigraphic (non-decompacted) thickness.

the thermal state of rocks driven by either compressional or extensional processes. Exhumation is simulated in a simplified way by prescribing perfectly vertical flow, and instantaneous erosion of the material points that reach the topographic surface, until the TPB reaches a final thickness of about 3 km, matching the actual value. The results show that for exhumation rates, between 2 and 10 mm/yr, the peak temperatures at the base of TPB fall rapidly in the range of 70–102°C after less than 0.2 Ma from the beginning of the experiments (Table 5; Figure 9a,e). Only the experiments using very high, geologically unrealistic, exhumation rates of 20 and 40 mm/yr maintain the temperature at the base of TPB above 100°C somewhat longer. In these models, temperatures close to the APAZ are expected to last no more than 1 Myr (Table 5; Figure 9a,e). Thus, all experiments show that exhumation alone could maintain peak temperatures close to the PAZ no longer than about 1 Ma, providing potential AFT ages at ca. 25 Ma at the base of TPB only assuming unreasonably fast exhumation rates.
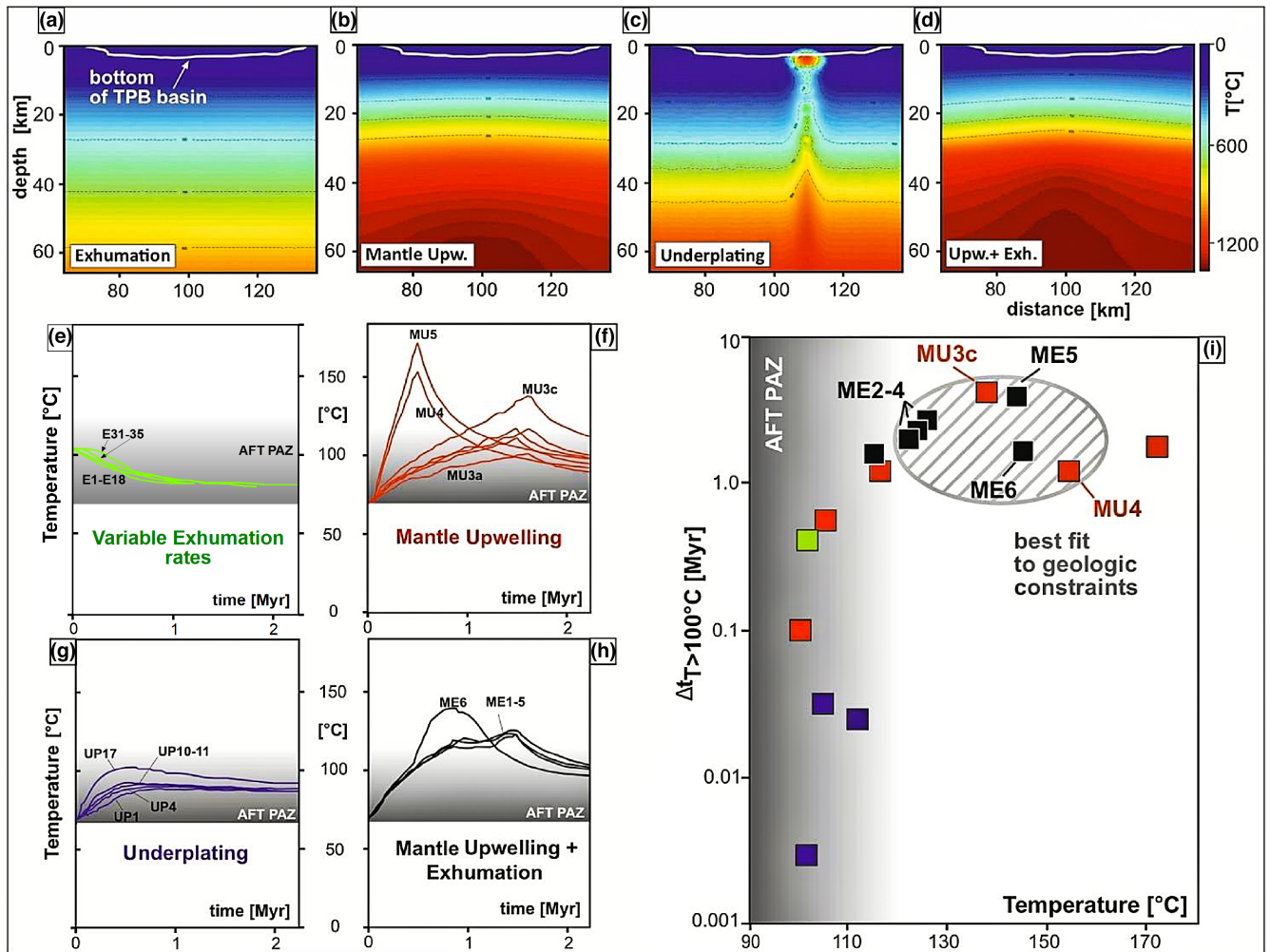
4.5.2 | Mantle upwelling

In the second set of scenarios, the upwelling of hot, partially molten asthenosphere leads almost systematically to a considerable increase in temperature at the base of a 60–90 km-thick lithosphere similar to those commonly

observed in collisional belts after the break-off of the oceanic plate (Davies & von Blanckenburg, 1995; Sizova et al., 2014). Two sub-sets of parametric experiments show that the duration and intensity of heating in the crustal region above the slab depend mostly on the size of the upwelling asthenosphere and the shallowest depth it reached (Table 5; Figure 9b,f). Specifically, the minimum depth of the asthenosphere appears to be relatively more effective in producing large and persistent thermal anomalies, which can last up to 4 Myr (exp. ME6 in Table 5). On the other hand, the expansion rate of the mantle thermal anomaly apparently has little or no effect on the geotherm of the uppermost crust (Figure 9i). In fact, relatively high temperatures in the range 100–170°C are obtained at the top of the asthenospheric window, at a depth of 80 km or shallower, regardless of its radius (Figure 9f; Table 5). These scenarios would explain the thermochronometric recorded at the base of the eastern TPB.

4.5.3 | Underplating

The occurrence of Oligocene-Miocene magmatism is evidenced by volcaniclastic deposits within the TPB sedimentary sequences and volcanoes relics in the Po Plain subsurface (Di Giulio et al., 2001; Fantoni et al., 1999; Ruffini et al., 1995). This suggests that the TPB thermal budget may also have been influenced by such volcanic

FIGURE 9 Experimental 2-D Thermal Modelling Results. (a) Pure Exhumation experiment (E). (b) Mantle upwelling experiment (MU). (c) Underplating experiment (UP) showing a magmatic body; (d) Mantle upwelling + Exhumation experiment (ME). Plots from e to h show the time–Temperature paths recorded at the base of the TPB from different experiments. (i) Temporal windows for heating calculated from the experiments with temperature >110°C at the base of the basin. For data and acronyms, refer to Table 5. Grey shaded area (AFT PAZ) represents the Partial Annealing Zone of the Apatite Fission Track system between 60–120°C.

activity. Experiments simulating magmatic underplating show that heating to temperatures over 500°C can be obtained close to the contact with the magmatic chamber for a wide range of melt injection rates and thickness of the magmatic layer (Figure 9c,g). These results agree with petrologic constraints provided by shallow crustal contact metamorphic aureoles, demonstrating the effectiveness of magmatism in modifying the local geothermal profile in the upper crust (Depine et al., 2008; Mitchell et al., 2014; Mori et al., 2017; Secchi et al., 2022). The effect of underplating is evaluated by experiments UP1-UP17 (Table 5) which use a finer grid with cell size of 50×50 m to portray the details of narrow contact metamorphic aureole. All high-resolution experiments show that heat rapidly vanishes a few meters (50–100 m) away from the intrusion (Figure 9c). Magmatic underplating experiments yield detectable modification of the steady-state geotherm only

for very large magmatic systems (20 km-long for 2–4 km-thick) composed of one thick intrusion or of laterally connected large bodies. The melt emplacement rate is also a critical factor for establishing a detectable thermal anomaly as only the experiments using >50 mm/yr produce temperature close to 100°C at the base of TPB (i.e. experiment UP17 in Table 5) (Figure 9g,i).

4.5.4 | Combined exhumation and mantle upwelling

A considerable heating is produced in the experiments combining exhumation with rates in the range 2–8 mm/year and mantle upwelling up to depths in the range 70–90 km. These simulations yielded temperatures at the base of the TPB in the range 110–140°C, albeit lasting

TABLE 5 Numerical results from thermal modelling experiments

	ID Experiments	Upper Lithosphere Thickness$_{metamorphic}$ (km)	Lower Lithosphere Thickness (km)	Lower Crust Composition	Model time duration (My)	Exhumation v_z (mm/yr)	Mantle upwelling L_b (km)	Z_b (km)	Underplating h_m (km)	Ω_m (mm/yr)	TPB T_{base} (°C)	T_{top} (°C)	$\Delta t_{T>100°C}$ (Myr)
Exhumation	E1	15	10	Granodiorite	4	2	0	0	0	0	87	48	/
	E2	18									86	46	/
	E3	21									87	46	/
	E4	25									87	47	/
	E10	18	8								85	46	/
	E12		12								80	58	/
	E15		16								78	51	/
	E18		20								73	51	/
	E21		12	Diorite							70	49	/
	E23			Gabbro							70	50	/
	E31				2.3	5					97	58	/
	E34				3.7	10					102	61	0.003
	E35				1.8	20					105	62	0.032
	E37				1.2	40					112	70	0.025
Mantle Upwellig	MU3				4.6	0	30	90			101	56	0.1
	MU3a				4.4		40				106	55	0.56
	MU3b				4.4		50				117	61	1.19
	MU3c				6.3		60	80			138	74	4.08
	MU4				3.2		40	70			155	91	1.2
	MU5				5.3			60			172	104	1.73
Underplating	UP1	20	10	Granodiorite	3.7	0	0	0	0.5	4.17	88	47	/
	UP4				1.56				1	11.11	90	48	/
	UP10				2.7				1	14.29	92	48	/
	UP11				2.7				1	22.22	92	49	/
	UP17				2.5				2	57.14	102	54	0.43
Mantle Upw. + Exhum.	ME1	18	12		3.5	2	40	90	0	0	116	62	1.57
	ME2				4.6	2	40	80			125	66	2.32
	ME3				3.9	2	40	70			126	67	2.61
	ME4				4	8	50	90			116	52	1.58
	ME5				4.6	8	50	80			123	64	1.99
	ME6				4.5	8	50	70			144	76	4.09

Note: V_z is the exhumation velocity. L_b and Z_b are the length and depth below the surface of the asthenospheric window. h_m is the size of the magmatic intrusion. Ω_m is the melt injection rate. In yellow are highlighted the results showing the best fit to geologic constraints. dt is the temporal windows for heating calculated from the experiments in Figure 9b with temperature >100°C at the base of the basin (Figure 9c). Best fits are imaged in Figure 9i.

for shorter time spans (1.5–4 Myr) compared to results from simulations with mantle upwelling alone (Table 5; Figure 9d,h,i). Therefore, a coupled effect of exhumation and mantle upwelling appears a good fit for the TPB thermal history recorded by AFT, capable of bringing the stratigraphically deepest and oldest sedimentary rocks to annealing temperatures without requiring unrealistically high exhumation rates or shallow asthenospheric plumes.

5 | DISCUSSION

Our study constrains the time–temperature history of the easternmost TPB, starting with the determination of maximum burial and related heating/cooling history and geothermal palaeo-gradient. The integration and discussion of these results with published data from all the TPB and its margin allow us to better resolve the Oligocene tectono-thermal evolution of the coupled orogen-basin system. Finally, numerical modelling helps to understand which geodynamic mechanisms were at play during the formation of the TPB.

5.1 | Burial and t–T history of the TPB

The analytical dataset allows us to constrain with confidence the temperature conditions of the TPB sequence through time and thus derive the relative palaeo-geothermal gradients. The restored thickness of the eastern TPB results in 2.3 ± 0.1 km depth at ca. 25 Ma, when the basal formation of the basin cooled from temperatures high enough to reset the AFT system. Fluid inclusion microthermometry on diagenetic minerals confirms that the lowermost samples experienced temperatures of ca. 130°C. Younger sedimentary units up-section progressively reached lower peak temperatures as recorded by partially to non-reset AFT ages and homogenization temperature of ca. 80°C. Inverse thermal history modelling confirms the possibility of an Oligocene temperature peak in the range of 100–120°C between 35 and 30 Ma (Figure 7) followed by cooling until present-day surface temperatures. This burial–temperature relation requires a relatively hot gradient of 45 ± 5°C/km characterizing the shallowest sedimentary cover (Figure 8).

Detrital AHe ages from the entire Oligo–Miocene sequence from western and eastern TPB are highly dispersed (Figure 10c) making the younger and shallower t–T path less straightforward to model and interpret. The AHe ages from units deposited between 35 and 20 Ma are reset, grouped between 10 and 16 Ma. Even though the dataset does not provide a narrow cluster of cooling ages, it proves that the Burdigalian–Tortonian upper units

have not been re-heated after deposition. Generally, the AHe system records rock cooling in the uppermost crust, below 90°C or at ca. 2–3 km depth (Farley, 2000, 2002), with age dispersion frequently encountered for a number of reasons (Brown et al., 2013; Fitzgerald et al., 2006; Flowers et al., 2009; Gautheron et al., 2009; Reiners & Farley, 2001). These may include analysis of few grains (Green & Duddy, 2018; Ketcham et al., 2018), partial and non-homogeneous reset and effects from radiation damage accumulation (i.e. rocks spent long time in the region of PRZ) (Flowers et al., 2009), hydrothermal fluid circulation (also present in the study area, Luijendik et al., 2020; Spooner et al., 2020) and local fault activity (Maino et al., 2020; Tagami, 2012).

Geothermal gradients in the range of 40–50°C/km are common in areas affected by deep magmatism, ocean–continent transition zones and incipient extensional domains (Brogi & Liotta, 2006; Vedova et al., 2001; Gholamrezaie et al., 2018; Girdler, 1970; Liao et al., 2014; Macgregor, 2020), whereas they are unusual in foreland or episutural basins. As an example, the present-day heat flux data from the western Po Plain and north-western Apennines are 60–70 mW/m², and the 120°C isotherm lies between 4.5 and 5.5 km depth, implying a regional geothermal gradient of 26°C/km (Pasquale et al., 2012; Pauselli et al., 2019). This current geothermal gradient is within the typical range of values on upper continental crust. Since the Miocene, the Po Plain region developed a 6–7 km-deep basin filled by water-saturated turbiditic sediments. These rocks are made by an alternation of sandstones and shales, both lithotypes with the low thermal conductivity with respect to crystalline rocks, limestone and evaporitic rocks (e.g. Midttømme & Roaldset, 1999; Tang et al., 2021). This implies a possible buffering or even insulating effect of the heat flow on the underlying rocks, preventing rapid heat loss. Thus, it is possible to infer that the Po basin may have been able to preserve an anomalous thermal structure at its base. In this case, it is reasonable to assume the palaeo-geothermal gradient in the Po region was higher during sediment deposition.

5.2 | Ligurian Alps thermal evolution

To test whether there is a relationship between the thermal evolution of the Tertiary-Piedmont Basin and its margin, it is necessary to look more closely at the thermal and exhumation history of the entire region. In particular, we take into account all the geo-thermochronometric data available in the literature from both the clastic TPB units and the metamorphic basement (Figures 4 and 10a for an overview).
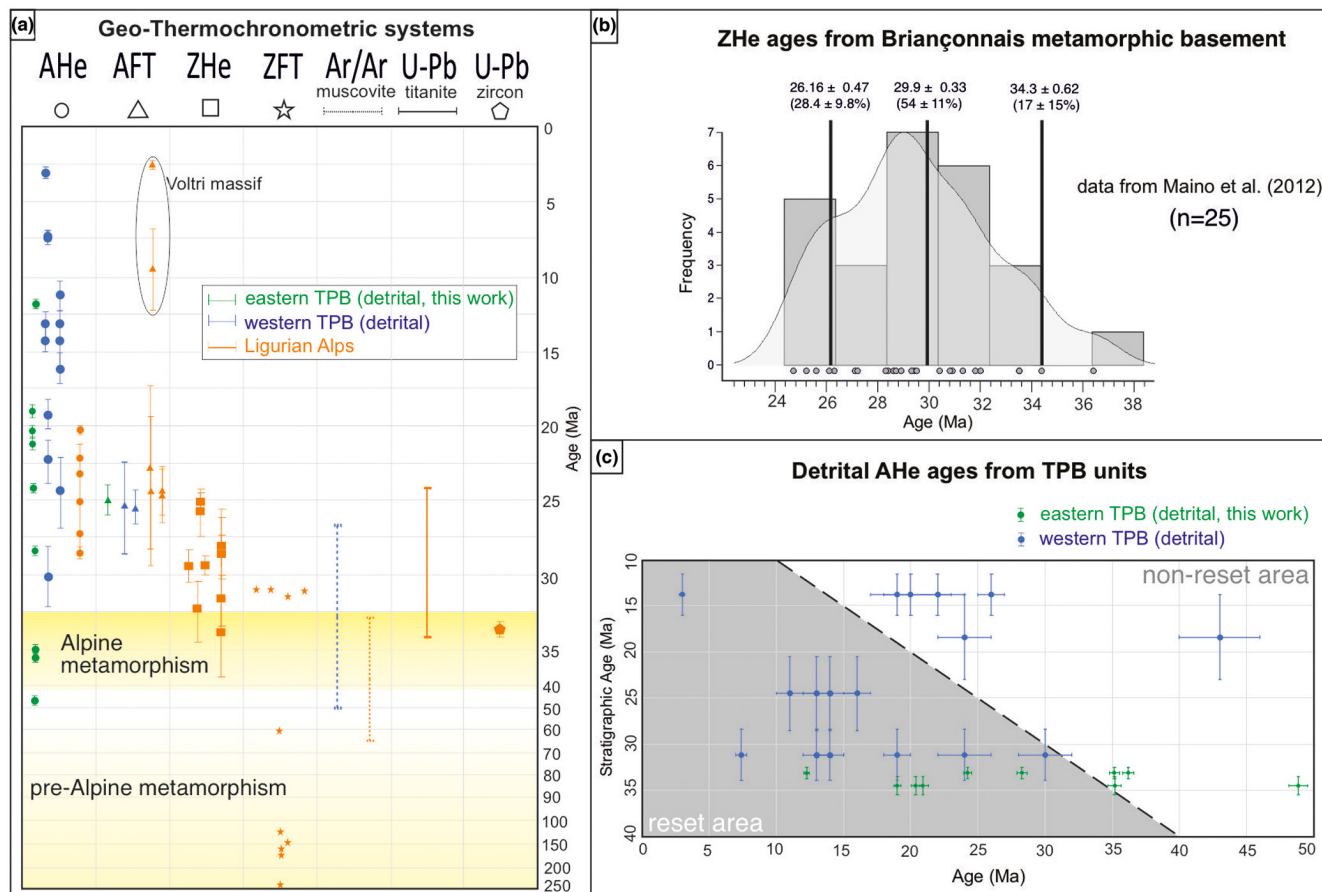
FIGURE 10 Geo-thermochronology dataset compilation. (a) Geo-thermochronometric systems ordered by increasing closure temperature from left to right. Grey arrow represents a general cooling trend. Data are also shown in map in Figure 4 and detailed in Table S1 in the supplemental material. (b) Probability density plot and histogram (bin width 2 Ma) of ZHe single grain ages from Briançonnais metamorphic basement sampled at the erosional boundary with the base of western TPB (data from Maino et al., 2012). (c) Lag-time plot of all AHe detrital ages from Oligo–Miocene TPB units showing high dispersion.

The Briançonnais massif yields a broad ZHe age distribution within a range of 36–24 Ma (Figure 10b) and could be explained as a result of an Oligocene partial overprint and not as the time of monotonic cooling through the Zhe PRZ up to the surface during the Alpine metamorphic peak, as previously suggested (Maino et al., 2012). These ages overlap the biostratigraphic age range of the basal western TPB deposits (Molare Fm.), which was derived from erosion of Briançonnais rocks at the surface supplying a source for the deposition of conglomerate (Barbieri et al., 2003; Capponi et al., 2009). A partial overprinting of the thermochronometric signature would also imply that the Briançonnais rocks were not cooled and exhumed at such extreme rates (>100°C/My) as was previously inferred (Barbieri et al., 2003; Carrapa et al., 2004; Federico et al., 2005; Maino et al., 2012).

Our AFT data from the eastern TPB indicate decoupled burial and thermal history models, the latter of which is characterized by a significant heating event between ca.

35 and 25 Ma, synchronous with the exhumation of the Ligurian Alps (Figure 11).

The higher temperature path of the Western and Ligurian Alps during the Alpine metamorphism predating TPB evolution may not be unambiguously interpreted. Several authors have suggested a non-homogeneous thermal resetting of higher temperature geochronometers based on the large spread of ZFT, spanning from ca. 31 to 180 Ma (Bernet et al., 2001; Decarlis et al., 2017; Vance, 1999) (Figures 10a and 11). This would also explain the occurrence of large range of U–Pb titanite and $^{40}Ar/^{39}Ar$ ages from both TPB pebbles and metamorphic basement, often overlapping the depositional ages of the basal TPB pebbly layer (Barbieri et al., 2003; Carrapa et al., 2004, 2016; Federico et al., 2005, 2007; Vignaroli et al., 2010).

Although this issue has received attention in the past because of its significant implications for the orogen dynamic (i.e. discerning between fast or slow exhumation
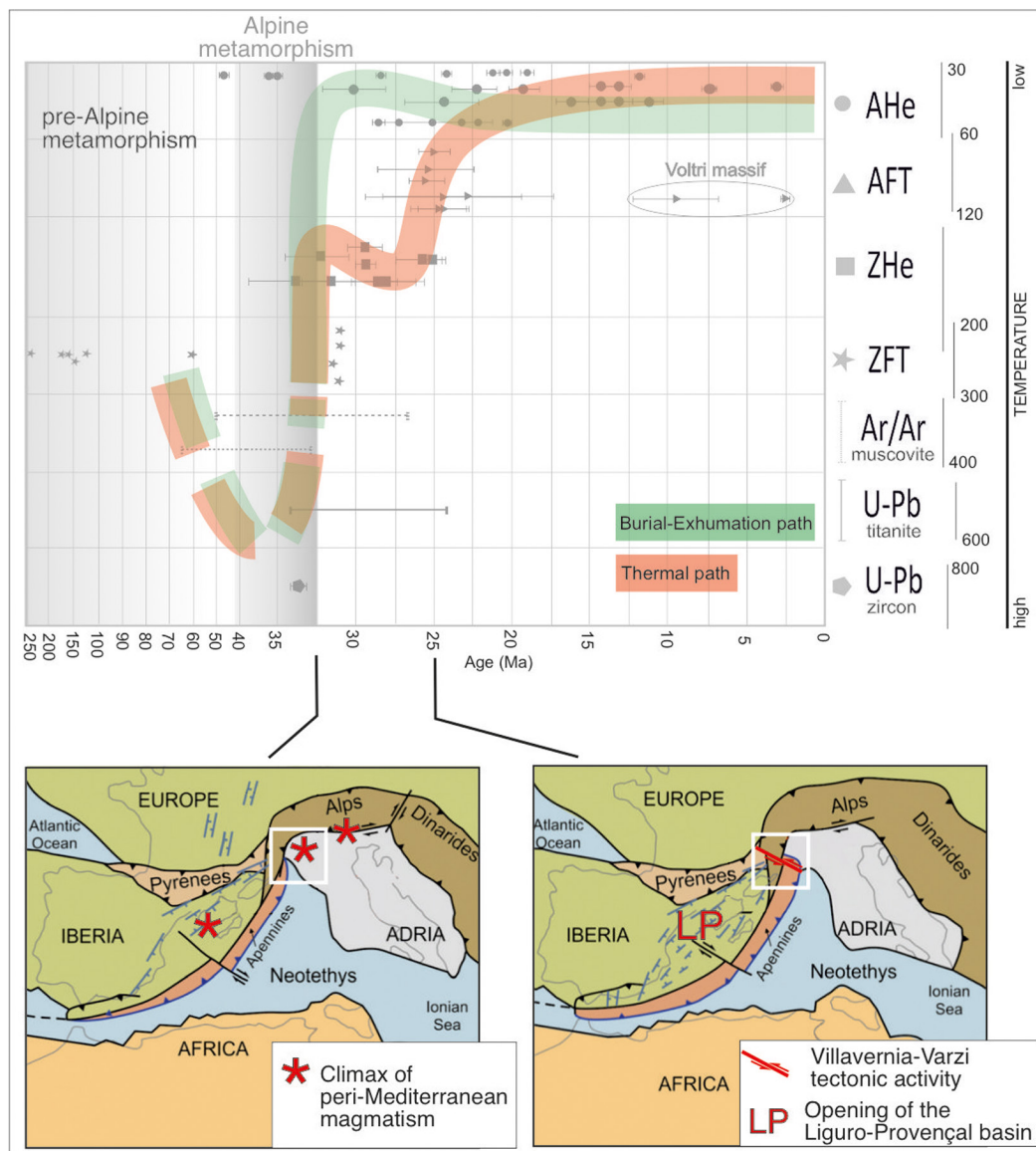
FIGURE 11 Burial-Exhumation and temperature indicative path of the Ligurian Alps and TPB. Temperature path is shown in red. Geo-thermochronometric data from Figure 10a, shown in map in Figure 4. Geodynamic maps modified from Handy et al. (2010) and Maino et al. (2013). White box borders the study area where the TPB developed.

dynamics), all geo-thermochonometric ages to date have been interpreted as indicative of very fast cooling and exhumation patterns. To solve this problem, additional geochronometric data are needed, coupled with compositional analysis to unravel possible variability of annealing kinetics.

5.3 | Possible heating mechanisms

An elevated geothermal gradient in the upper crust may result from a variety of processes. These include advection of hot rock units, circulation of hot fluids/melts and shear heating (e.g. Burg & Gerya, 2005; Depine et al., 2008; Duprat-Oualid et al., 2015; Maino et al., 2015,

2020), which can superpose to produce a localized thermal peak. In the Alpine context, regional heating is largely coeval with the transition from subduction to collision (Carminati et al., 2012; Ford et al., 2006; Rosenbaum & Lister, 2005). We have investigated three processes which might account for the large-scale high geothermal gradient needed to explain the Oligocene thermochronological record of Western and Ligurian Alps: (i) fast exhumation of thickened crust driven by either compressional or extensional tectonics (Duprat-Oualid et al., 2015); (ii) magmatic/volcanic activity driven by underplating of hot, mantle-derived melts (Mori et al., 2017); (iii) mantle upwelling due either to slab rollback or break-off (e.g. Davies & von Blanckenburg, 1995). The results obtained from 2-D thermal numerical modelling allow us to discuss the

effectiveness of these different mechanisms, and the relative influence of various parameters such as crustal exhumation rates, depth and size of asthenospheric upwelling, thickness and advection rates of magmatic systems. From the first set of experiments, we argue that fast exhumation alone cannot account for the observed temperature pattern. In the absence of any other cooperative mechanism, exhumation rates >20–40 mm/yr would be required to increase the temperature of TPB to about 100°C. These extreme values exceed, by more than one order of magnitude, the maximum exhumation rates of the Western Alps (0.6–0.8 mm/yr; Fox et al., 2015, 2016). Magmatism, associated with protracted volcanic activity, can significantly heat the uppermost crust and sedimentary basins (Annen, 2011; Annen, et al., 2006; Secchi et al., 2022). The occurrence of two andesitic volcanic complexes a few km north of the TPB (Mortara-Lacchiarella complexes, see Figure 1c for location) apparently supports this model, provided that some sufficiently thick, still undetected magmatic bodies are emplaced within the TPB or close to its base. The minimum thickness required of the intrusion/volcanic complex to reproduce the temperature pattern of TPB exceeds 1 km, which corresponds to a maximum thickness of Mortara volcanic centre recovered by well log data (Mortara 1 well), although the edifice thins to 20 m in a 15 km radius, as recorded in the Garlasco 1 well (Dalla et al., 1992; Di Giulio et al., 2001; Fantoni et al., 1999; Pieri & Groppi, 1981). However, the second set of numerical experiments rule out the hypothesis of magmatic heating as, regardless of the dimension of the volcanic body, our analytical results cannot reproduce the observed temperature pattern unless using unrealistically high melt injection rates of >50 mm/yr (Annen, 2011; Annen, et al., 2006; Albert et al., 2020).

The last two sets of simulations indicate that a deep thermal input from the asthenospheric mantle, possibly combined with exhumation, is required to reproduce the observed temperature pattern in the lower TPB. Contrary to the underplating experiments, mantle upwelling likely produces a wide and persistent thermal anomaly in the uppermost crust for most configurations of the asthenospheric window (Figure 1b and modelled as in Figure 5). These mantle-related thermal anomalies can support temperatures >120°C for a few million years, thus explaining the extensive resetting of AFT and high fluid inclusion homogenization temperatures in the lowermost TPB.

The post-orogenic, mantle-related thermal anomaly here described may be related to the Oligocene inception of the Liguro-Provençal rifting (Figure 11; Bache et al., 2010, 2020; Jolivet et al., 2015; Séranne, 1999; Speranza et al., 2002; Vignaroli et al., 2008; Vignaroli et al., 2010). The related stress-field produced the activation of trans-extensional faults in the Ligurian Alps-TPB,

coinciding with the switch from an extensional to a left-lateral transtensional regime (Maino et al., 2013), while the Sestri-Voltaggio and Villalvernia-Varzi lines acted as strike-slip faults (see Figure 1c, Capponi et al., 2009; Di Giulio & Galbiati, 1995; Federico et al., 2009, 2016, 2020; Felletti, 2002) accommodating the differential motion of the west-directed Alps and northeast verging of Apennine chain (Figure 11). This extensional setting represents the surface manifestation of lithospheric stretching driven by the opposite motion of the Alps and Apennines, which favoured the asthenospheric upwelling. During the Miocene, the Liguro-Provençal rift basin completed its opening, with the continental lithosphere complete break up and formation of new oceanic crust between ca. 20 and 15 Ma (Séranne, 1999; Speranza et al., 2002).

At local scale, our new fluid inclusion homogenization temperatures (Figure 6a), along with inverse thermal models (Figure 8), indicate that the TPB base experienced temperatures quickly decreasing from >100°C (TPB1) to ca. 80–90°C (TPB7) in a few hundreds of meters of vertical distance (Figure 3b). Moreover, all up-section samples (TPB8 to 12), although proximal to the partially reset TPB7, yield non-reset AFT ages and fluid inclusion homogenization temperatures at 80°C, consistent through the shallowest units. We suggest such a non-typical, that is, non-linear, trend is likely a result of geological complexity, and we propose two processes able to produce the non-linear geothermal gradient in the basin. Firstly, geothermal heat from the upper continental crust is preferentially retained in highly conductive crystalline rocks, like the metamorphic basement, and is not efficiently and equally transferred into less conductive sedimentary rocks (e.g. Vedova et al., 2001; Pasquale et al., 2012). Consequently, TPB basal samples are more susceptible to heating from a deep source than their up-section counterparts. Secondly, we can interpret the fairly constant fluid inclusion homogenization temperatures in the middle-upper sedimentary sequence as the result of hydrothermal fluids that buffered the thermal changes. Given the proximal location of the samples to the Villalvernia-Varzi line, it is also reasonable to assume its tectonic activity to have contributed to the fluid–rock interaction.

6 | CONCLUSIONS

Our study shows that elevated temperatures post-deposition recorded by fluid inclusion microthermometry and low-T thermochronometers in the TPB cannot be explained by sedimentary burial alone. Our findings support a post-depositional heating temperature of ca. 100–120°C accomplished at shallow depth (ca. 2.3 km)

between ca. 35 and 25 Ma, followed by slow cooling from ca. 20 Ma to recent time. When combined, our data show that a geothermal gradient of $45 \pm 5°C/km$ is required. 2-D numerical simulations used to evaluate different geodynamic processes indicate that volcanism or fast exhumation alone cannot explain the observed thermal signal. Significant mantle upwelling is required to account for the measured hot and shallow thermal signal. Due to the purely thermal nature of the experiments, no attempt was made to discriminate slab rollback or break-off, as both mechanisms likely produce similar heating signals to an asthenosphere plume. The post-orogenic thermal anomaly constrained by this study is coeval with the opening and developing of the Liguro-Provençal back-arc basin, and hence consistent with mantle upwelling processes.

CONFLICT OF INTEREST
The authors declare that they have no known competing financial interests or personal relationships that could have appeared to influence the work reported in this paper.

PEER REVIEW
The peer review history for this article is available at https://publons.com/publon/10.1111/bre.12752.

DATA AVAILABILITY STATEMENT
The data that support the findings of this study are openly available in Interdisciplinary Earth Data Alliance (IEDA) at https://doi.org/10.26022/IEDA/111829, reference number IEDA/111829.

ORCID
Chiara Amadori https://orcid.org/0000-0002-7220-442X
Matteo Maino https://orcid.org/0000-0001-8766-8027
Gilby Jepson https://orcid.org/0000-0003-0151-3062
Andrea Di Giulio https://orcid.org/0000-0002-0893-759X

REFERENCES

Albert, H., Larrea, P., Costa, F., et al. (2020). Crystals reveal magma convection and melt transport in dyke-fed eruptions. *Scientific Reports*, *10*, 11632. https://doi.org/10.1038/s41598-020-68421-4

Allen, P. A., & Allen, J. R. (2013). *Basin analysis: Principles and application to petroleum play assessment* (3rd ed.). Blackwell Scientific. 619 pp. ISBN 978-0-470-67376

Amadori, C., Garcia-Castellanos, D., Toscani, G., Sternai, P., Fantoni, R., Ghielmi, M., & Di Giulio, A. (2018). Restored topography of the Po Plain-Northern Adriatic Region during the Messinian base-level drop—Implications for the physiography and compartmentalization of the paleo-Mediterranean basin. *Basin Research*, *30*(6), 1247–1263. https://doi.org/10.1111/bre.12302. hdl:11571/1221647

Amadori, C., Ghielmi, M., Mancin, N., & Toscani, G. (2020). The evolution of a coastal wedge in response to Plio-Pleistocene climate change: The Northern Adriatic cases. *Marine and Petroleum Geology*, *122*, 104675. https://doi.org/10.1016/j.marpetgeo.2020.104675. hdl:11571/1346103

Amadori, C., Toscani, G., Di Giulio, A., Maesano, F. E., D'Ambrogi, C., Ghielmi, M., & Fantoni, R. (2019). From cylindrical to non-cylindrical foreland basin: Pliocene–Pleistocene evolution of the Po Plain–Northern Adriatic basin (Italy). *Basin Research*, *31*(5), 991–1015. https://doi.org/10.1111/bre.12369

Andreoni, G., Galbiati, B., Maccabruni, A., & Vercesi, P. L. (1981). Stratigrafia e paleogeografia dei depositi oligocenici sup.-miocenici inf. nell'estremità orientale del Bacino Ligure-Piemontese. *Rivista Italiana di Paleontologia e Stratigrafia*, *87*, 245–282.

Annen, C. (2011). Implications of incremental emplacement of magma bodies for magma differentiation, thermal aureole dimensions and plutonism–volcanism relationships. *Tectonophysics*, *500*(1-4), 3–10. https://doi.org/10.1016/j.tecto.2009.04.010

Annen, C., Scaillet, B., & Sparks, R. (2006). Thermal constraints on the emplacement rate of a large intrusive complex: The Manaslu leucogranite, Nepal Himalaya. *Journal of Petrology*, *47*(1), 71–95. https://doi.org/10.1093/petrology/egi068

Armstrong, P. A. (2005). Thermochronometers in sedimentary basins. *Reviews in Mineralogy and Geochemistry*, *58*(1), 499–525.

Armstrong, P. A., & Chapman, D. S. (1998). Beyond surface heat flow: An example from a tectonically active sedimentary basin. *Geology*, *26*(2), 183–186.

Bache, F., Olivet, J. L., Gorini, C., Aslanian, D., Labails, C., & Rabineau, M. (2010). Evolution of rifted continental margins: The case of the Gulf of Lions (Western Mediterranean Basin). *Earth and Planetary Science Letters*, *292*(3–4), 345–356. https://doi.org/10.1016/j.epsl.2010.02.001

Bache, F., Olivet, J. L., Gorini, C., Aslanian, D., & Rabineau, M. (2020). Evolution of rifted continental margins: The case of the Gulf of Lions (Western Mediterranean Basin). *Earth and Planetary Science Letters*, *292*(3–4), 345–356. https://doi.org/10.1016/j.epsl.2010.02.001

Balestrieri, M. L., Abbate, E., & Bigazzi, G. (1996). Insights on the thermal evolution of the Ligurian Apennines (Italy) through fission-track analysis. *Journal of the Geological Society, London*, *153*, 419–425.

Barbieri, C., Carrapa, B., Di Giulio, A., Wijbrans, J., & Murrell, G. R. (2003). Provenance of Oligocene synorogenic sediments of the

Ligurian Alps (NW Italy): Inferences on belt age and cooling history. *International Journal of Earth Sciences*, *92*(5), 758–778.

Bernet, M., Zattin, M., Garver, J. I., Brandon, M. T., & Vance, J. A. (2001). Steady state exhumation of the European Alps. *Geology*, *29*, 35–38.

Bertotti, G., Mosca, P., Juez, J., Polino, R., & Dunai, T. (2006). Oligocene to present kilometres scale subsidence and exhumation of the Ligurian Alps and the Tertiary Piedmont Basin (NW Italy) revealed by apatite (U–Th)/He thermochronology: Correlation with regional tectonics. *Terra Nova*, *18*(1), 18–25.

Boccaletti, M., Coli, M., & Napoleone, G. (1980). Landsat lineation pattern in the Apennines and its geodynamic significance. *Modern Geology*, *7*(2), 95–103.

Bonini, L., Dallagiovanna, G., & Seno, S. (2010). The role of pre-existing faults in the structural evolution of thrust systems: Insights from the Ligurian Alps (Italy). *Tectonophysics*, *480*(1–4), 73–87.

Brogi, A., & Liotta, D. (2006). Understanding the crustal structures of southern Tuscany: The contribution of the CROP18 project. *Bollettino di Geofisica Teorica ed Applicata*, *47*(3), 401–423.

Brown, R. W., Beucher, R., Roper, S., Persano, C., Stuart, F., & Fitzgerald, P. (2013). Natural age dispersion arising from the analysis of broken crystals. Part I: Theoretical basis and implications for the apatite (U-Th)/He thermochronometer. *Geochimica et Cosmochimica Acta*, *122*, 478–497. https://doi.org/10.1016/j.gca.2013.05.041

Burg, J. P., & Gerya, T. V. (2005). The role of viscous heating in Barrovian metamorphism of collisional orogens: Thermomechanical models and application to the Lepontine Dome in the Central Alps. *Journal of Metamorphic Geology*, *23*(2), 75–95. https://doi.org/10.1111/j.1525-1314.2005.00563.x

Capó, A., & Garcia, C. (2019). Basin filling evolution of the central basins of Mallorca since the Pliocene. *Basin Research*, *31*(5), 948–966. https://doi.org/10.1111/bre.12352

Capponi, G., & Crispini, L. (2002). Structural and metamorphic of alpine tectonics in the Voltri Massif (Ligurian Alps, North-Western Italy). *Eclogae Geologicae Helvetiae*, *95*(1), 31–42.

Capponi, G., Crispini, L., Federico, L., & Malatesta, C. (2016). Geology of the eastern Ligurian Alps: A review of the tectonic units. *Italian Journal of Geosciences*, *135*(1), 157–169. https://doi.org/10.3301/IJG.2015.06

Capponi, G., Crispini, L., Federico, L., Piazza, M., & Fabbri, B. (2009). Late Alpine tectonics in the Ligurian Alps: Constraints from the Tertiary Piedmont Basin conglomerates. *Geological Journal*, *44*(2), 211–224. https://doi.org/10.1002/gj.1140

Carlson, W. D., Donelick, R. A., & Ketcham, R. A. (1999). Variability of apatite fission-track annealing kinetics: I. Experimental results. *American Mineralogist*, *84*(9), 1213–1223. https://doi.org/10.2138/am-1999-0901

Carminati, E., Lustrino, M., & Doglioni, C. (2012). Geodynamic evolution of the central and western Mediterranean: Tectonics vs. igneous petrology constraints. *Tectonophysics*, *579*, 173–192. https://doi.org/10.1016/j.tecto.2012.01.026

Carrapa, B., Bertotti, G., & Krijgsman, W. (2003). Subsidence, stress regime and rotation(s) of a tectonically active sedimentary basin within the western Alpine Orogen: The Tertiary Piedmont Basin (Alpine domain, NW Italy). *Geological Society, London, Special Publications*, *208*(1), 205–227.

Carrapa, B., Di Giulio, A., Mancin, N., Stockli, D., Fantoni, R., Hughes, A., & Gupta, S. (2016). Tectonic significance of Cenozoic exhumation and foreland basin evolution in the Western Alps. *Tectonics*, *35*(8), 1892–1912. https://doi.org/10.1002/2016TC004132

Carrapa, B., Di Giulio, A., & Wijbrans, J. (2004). The early stages of the alpine collision: An image derived from the upper Eocene–lower Oligocene record in the Alps–Apennines junction area. *Sedimentary Geology*, *171*(1–4), 181–203.

Carrapa, B., & Garcia-Castellanos, D. (2005). Western Alpine back-thrusting as subsidence mechanism in the Tertiary Piedmont Basin (western Po Plain, NW Italy). *Tectonophysics*, *406*(3–4), 197–212.

Casini, L. (2012). A MATLAB-derived software (geothermMOD1.2) for one-dimensional thermal modelling, and its application to the Corsica-Sardinia batholith. *Computers and Geosciences*, *45*, 82–86. https://doi.org/10.1016/j.cageo.2011.10.020

Casini, L., & Maino, M. (2018). 2D-thermo-mechanical modelling of spatial P-T variations in heterogeneous shear zones. *Italian Journal of Geosciences*, *137*(2), 272–282. https://doi.org/10.3301/IJG.2018.13

Casini, L., Puccini, A., Cuccuru, S., Maino, M., & Oggiano, G. (2013). GEOTHERM: A finite difference code for testing metamorphic P-T-t paths and tectonic models. *Computers and Geosciences*, *59*, 171–180. https://doi.org/10.1016/j.cageo.2013.05.017

Castellarin, A. (2001). Alps-Apennines and Po Plain-frontal Apennines relations. In G. B. Vai & I. P. Martini (Eds.), *Anatomy of an Orogen: The Apennines and adjacent Mediterranean basins* (pp. 177–195). Springer Netherlands. https://doi.org/10.1007/978-94-015-9829-3_13

Cavanna, F., Di Giulio, A., Galbiati, B., Mosna, S., Perotti, C. R., & Pieri, M. (1989). Carta geologica dell'estremità orientale del Bacino Terziario Ligure-Piemontese. *Atti Ticinensi Di Scienze Della Terra*, *32*(1).

Ceriani, A., Arboit, F., Di Giulio, A., Decarlis, A., Steuber, T., Amadori, C., & Al, S. A. (2021). The influence of fragile deformation on the deposition of seep-carbonates: A case study in the South Alps-Apennines tectonic knot. *Basin Research.*, *34*, 555–569. https://doi.org/10.1111/bre.12630

Ceriani, A., Di Giulio, A., Goldstein, R. H., & Rossi, C. (2002). Diagenesis associated with cooling during burial: An example from Lower Cretaceous reservoir sandstones (Sirt Basin, Libya). *AAPG Bulletin*, *86*(9), 1573–1591.

Ceriani, A., Di Giulio, A., Fantoni, R., & Scotti, P. (2006). Cooling in rifting sequences during increasing burial depth due to heat flow decrease. *Terra Nova*, *18*(5), 365–371.

Cibin, U., Di Giulio, A., & Martelli, L. (2003). Oligocene-early Miocene tectonic evolution of the northern Apennines (north-western Italy) traced through provenance of piggy-back basin fill successions. *Geological Society, London, Special Publications*, *208*(1), 269–287.

Corrado, S., Schito, A., Romano, C., Grigo, D., Poe, B. T., Aldega, L., Caricchi, C., di Paolo, L., & Zattin, M. (2020). An integrated platform for thermal maturity assessment of polyphase, long-lasting sedimentary basins, from classical to brand-new thermal parameters and models: An example from the on-shore Baltic Basin (Poland). *Marine and Petroleum Geology*, *122*, 104547. https://doi.org/10.1016/j.marpetgeo.2020.104547

Crispini, L., Federico, L., Capponi, G., & Spagnolo, C. (2009). Late orogenic transpressional tectonics in the «Ligurian knot». *Bollettino Della Società Geologica Italiana*, *128*(2), 433–441.

Dalla, S., Rossi, M. E., Orlando, M., Visentin, C., Gelati, R., Gnaccolini, M., Papani, G., Belli, A., Biffi, U., & Catrullo, D. (1992). Late Eocene-Tortonian tectono-sedimentary evolution in the western part of the Padan Basin, northern Italy. *Paleontology and Evolution*, *24–25*, 341–362.

D'Atri, A., Dela Pierre, F., Ruffini, R., Novaretti, A., Cosca, M. A., & Hunziker, J. C. (2001). Calcareous plankton biostratigraphy and $^{40}Ar/^{39}Ar$ dating of miocene volcaniclastic layers from Monferrato (NW Italy). *Eclogae Geologicae Helvetiae*, *94*(2), 137–144. https://doi.org/10.5169/seals-168883

Davies, J. H., & von Blanckenburg, F. (1995). Slab breakoff: A model of lithosphere detachment and its test in the magmatism and deformation of collisional orogens. *Earth and Planetary Science Letters*, *129*(1–4), 85–102. https://doi.org/10.1016/0012-821X(94)00237-S

de Voogd, B., Nicolich, R., Olivet, J. L., Fanucci, F., Burrus, J., & Mauffret, A. (1991). First deep seismic reflection transect from the Gulf of Lions to Sardinia (ECORS-crop profiles in Western Mediterranean). *American Geophysical Union (AGU)*, *22*, 265–274. https://doi.org/10.1029/gd022p0265

Decarlis, A., Beltrando, M., Manatschal, G., Ferrando, S., & Carosi, R. (2017). Architecture of the distal Piedmont-Ligurian rifted margin in NW Italy: Hints for a flip of the rift system polarity. *Tectonics*, *36*, 2388–2406. https://doi.org/10.1002/2017TC004561

DeCelles, G., & Giles, K. N. (1996). Foreland basin systems. *Basin Research*, *8*, 105–123.

Depine, G. V., Andronicos, C. L., & Phipps-Morgan, J. (2008). Near-isothermal conditions in the middle and lower crust induced by melt migration. *Nature*, *452*(7183), 80–83. https://doi.org/10.1038/nature06689

Di Giulio, A. (1991). Detritismo della parte orientale del Bacino Terziario Piemontese durante l'Eocene-Oligocene: composizione delle arenarie ed evoluzione tettono-stratigrafica. *Atti Ticinensi Di Scienze Della Terra*, *34*, 21–22.

Di Giulio, A., Amadori, C., Mueller, P., & Langone, A. (2020). The role of the down-bending plate as detrital source in convergent systems revealed by U-Pb dating of zircon grains: Insights from southern Andes and Western Italian Alps. *Minerals—Special Issue Detrital Mineral U/Pb Age Dating and Geochemistry of Magmatic Products in Basin Sequences: State of the Art and Progress*, *10*, 623. https://doi.org/10.3390/min10070632. hdl:11571/1343508

Di Giulio, A., Carrapa, B., Fantoni, R., Gorla, L., & Valdisturlo, A. (2001). Middle Eocene to Early Miocene sedimentary evolution of the western Lombardian segment of the South Alpine foredeep (Italy). *International Journal of Earth Sciences*, *90*(3), 534–548. https://doi.org/10.1007/s005310000186

Di Giulio, A., & Galbiati, B. (1995). Interaction between tectonics and deposition into an episutural basin in the Alps-Apennine knot. *Atti Convegno Rapporti Alpi–Appennino*, *14*, 113–128.

Di Giulio, A., Grigo, D., Zattin, M., Amadori, C., Consonni, A., Nicola, C., Ortenzi, A., Scotti, P., & Tamburelli, S. (2021). Diagenetic history vs. thermal evolution of Paleozoic and Triassic reservoirs rocks in the Ghadames-Illizi Basin (Algeria-Tunisia-Lybia). *Marine and Petroleum Geology*, *127*, 104979. https://doi.org/10.1016/j.marpetgeo.2021.104979

Di Giulio, A., Marini, M., Felletti, F., Patacci, M., Rossi, M., & Amadori, C. (2019). Control exerted by collisional tectonics on basin topography and depositional styles: The Tertiary

Piedmont Basin in the Alps-Apennines junction (NW Italy). In M. Vigliotti, M. Tropeano, V. Pascucci, D. Ruberti, & L. Sabato (Eds.), *Field Trips—GUIDE BOOK, 34th IAS Meeting of Sedimentology, Rome (Italy) September 10–13 2019, Post-Meeting Field Trip B2* (pp. 303–332). Associazione Italiana di Geologia del Sedimentario—GeoSed ISBN 978-88-944576-0-5.

Di Stefano, R., Bianchi, I., Ciaccio, M. G., Carrara, G., & Kissling, E. (2011). Three-dimensional Moho topography in Italy: New constraints from receiver functions and controlled source seismology. *Geochemistry, Geophysics, Geosystems*, *12*, Q09006. https://doi.org/10.1029/2011GC003649

Donelick, R. A. (1993). *A method of fission track analysis utilizing bulk chemical etching of apatite*. (U.S. Patent No. 5,267,274).

Donelick, R. A., O'Sullivan, P. B., & Ketcham, R. A. (2005). Apatite fission-track analysis. *Reviews in Mineralogy and Geochemistry*, *58*(1), 49–94. https://doi.org/10.2138/rmg.2005.58.3

Duprat-Oualid, S., Yamato, P., & Schmalholz, S. M. (2015). A dimensional analysis to quantify the thermal budget around lithospheric-scale shear zones. *Terra Nova*, *27*(3), 163–168. https://doi.org/10.1111/ter.12144

Ehlers, T. A., & Farley, K. A. (2003). Apatite (U-Th)/He thermochronometry: Methods and applications to problems in tectonic and surface processes. *Earth and Planetary Science Letters*, *206*(1–2), 1–14. https://doi.org/10.1016/S0012-821X(02)01069-5

Fantoni, R., Bersezio, R., Forcella, F., Gorla, L., Mosconi, A., & Picotti, V. (1999). New dating of the Tertiary magmatic products of the central Southern Alps. Bearings on the interpretation of Alpine tectonic history. *Memorie Di Scienze Geologiche*, *51*(1), 47–61.

Farley, K. A. (2000). Helium diffusion from apatite; general behavior as illustrated by Durango fluorapatite. *Journal of Geophysical Research*, *105*, 2903–2914.

Farley, K. A. (2002). (U-Th)/He dating: Techniques, calibrations, and applications. *Reviews in Mineralogy and Geochemistry*, *47*(1), 819–844. https://doi.org/10.2138/rmg.2002.47.18

Federico, L., Capponi, G., Crispini, L., Scambelluri, M., & Villa, I. M. (2005). $^{39}Ar/^{40}Ar$ dating of high-pressure rocks from the Ligurian Alps: Evidence for a continuous subduction-exhumation cycle. *Earth and Planetary Science Letters*, *240*(3–4), 668–680. https://doi.org/10.1016/j.epsl.2005.09.062

Federico, L., Crispini, L., Dabove, G. M., Piazza, M., & Capponi, G. (2016). Stratigraphic vs structural contacts in a late orogenic basin: The case of the Tertiary Piedmont Basin in the Sassello area (Ligurian Alps, Italy). *Journal of Maps*, *12*(5), 959–967.

Federico, L., Crispini, L., Scambelluri, M., & Capponi, G. (2007). Ophiolite mélange zone records exhumation in a fossil subduction channel. *Geology*, *35*(6), 499–502.

Federico, L., Maino, M., Capponi, G., & Crispini, L. (2020). Paleo-depth of fossil faults estimated from paleostress state: Applications from the Alps and the Apennines (Italy). *Journal of Structural Geology*, *140*, 104152. https://doi.org/10.1016/j.jsg.2020.104152

Federico, L., Spagnolo, C., Crispini, L., & Capponi, G. (2009). Fault-slip analysis in the metaophiolites of the Voltri Massif: Constraints for the tectonic evolution at the Alps/Apennine boundary. *Geological Journal*, *44*(2), 225–240. https://doi.org/10.1002/gj.1139

Felletti, F. (2002, August). Complex bedding geometries and facies associations of the turbiditic fill of a confined basin in a transpressive setting (Castagnola Fm., Tertiary Piedmont

Basin, NW Italy). *Sedimentology*, 49(4), 645–667. https://doi. org/10.1046/j.1365-3091.2002.00467.x

Felletti, F. (2004a). Spatial variability of Hurst statistics in the Castagnola formation, Tertiary Piedmont Basin, NW Italy: Discrimination of sub-environments in a confined turbidite system. *Geological Society, London, Special Publications*, 222(1), 285–305.

Felletti, F. (2004b). Statistical modelling and validation of correlation in turbidites: An example from the Tertiary Piedmont Basin (Castagnola Fm., Northern Italy). *Marine and Petroleum Geology*, 21(1), 23–39.

Festa, A., Fioraso, G., Bissacca, E., & Petrizzo, M. R. (2015). Geology of the Villalvernia—Varzi line between Scrivia and Curone valleys (NW Italy). *Journal of Maps*, 11(1), 39–55. https://doi. org/10.1080/17445647.2014.959569

Fitzgerald, P. G., Baldwin, S. L., Webb, L. E., & O'Sullivan, P. B. (2006). Interpretation of (U-Th)/He single grain ages from slowly cooled crustal terranes: A case study from the Transantarctic Mountains of southern Victoria Land. *Chemical Geology*, 225(1–2), 91–120. https://doi.org/10.1016/j.chemg eo.2005.09.001

Flowers, R. M., Ketcham, R. A., Shuster, D. L., & Farley, K. A. (2009). Apatite (U-Th)/He thermochronometry using a radiation damage accumulation and annealing model. *Geochimica et Cosmochimica Acta*, 73(8), 2347–2365.

Foeken, J., Dunai, T., Bertotti, G., & Andriessen, P. (2003). Late Miocene to present exhumation in the Ligurian Alps (SW Alps) with evidence for accelerated denudatio during the Messinian Salinity Crisis. *Geology*, 31, 797–800.

Ford, M., Duchêne, S., Gasquet, D., & Vanderhaeghe, O. (2006). Two-phase orogenic convergence in the external and internal SW Alps. *Journal of the Geological Society*, 163(5), 815–826. https:// doi.org/10.1144/0016-76492005-034

Fox, M., Herman, F., Kissling, E., & Willett, S. D. (2015). Rapid exhumation in the Western Alps driven by slab detachment and glacial erosion. *Geology*, 43, 379–382.

Fox, M., Herman, F., Willett, S. D., & Schmid, S. M. (2016). The exhumation history of the European Alps inferred from linear inversion of thermochronometric data. *American Journal of Science*, 316, 505–541. https://doi.org/10.2475/06.2016.01

Galbraith, R. F., & Green, P. F. (1990). Estimating the component ages in a finite mixture. *International Journal of Radiation Applications and Instrumentation. Part D. Nuclear Tracks and Radiation Measurements*, 17(3), 197–206.

Galbraith, R. F., & Laslett, G. M. (1993). Statistical models for mixed fission track ages. *Nuclear Tracks and Radiation Measurements*, 21, 459–470.

Gallagher, K. (2012). Transdimensional inverse thermal history modeling for quantitative thermochronology. *Journal of Geophysical Research: Solid Earth*, 117, B02408. https://doi. org/10.1029/2011JB008825

Gallagher, K., Stephenson, J., Brown, R., Holmes, C., & Fitzgerald, P. (2005). Low temperature thermochronology and modeling strategies for multiple samples 1: Vertical profiles. *Earth and Planetary Science Letters*, 237(1–2), 193–208. https://doi. org/10.1016/j.epsl.2005.06.025

Gattacceca, J., Deino, A., Rizzo, R., Jones, D. S., Henry, B., Beaudoin, B., & Vadeboin, F. (2007). Miocene rotation of Sardinia: New paleomagnetic and geochronological constraints and geodynamic implications. *Earth and Planetary Science Letters*, 258(3–4), 359–377. https://doi.org/10.1016/j.epsl.2007.02.003

Gautheron, C., Tassan-Got, L., Barbarand, J., & Pagel, M. (2009). Effect of alpha-damage annealing on apatite (U-Th)/He thermochronology. *Chemical Geology*, 266(3), 157–170. https://doi. org/10.1016/j.chemgeo.2009.06.001

Gelati, R. (1977). La successione eo-oligocenica di Garbagna (Alessandria) al margine orientale del Bacino Terziario Ligure Piemontese. *Rivista Italiana di Paleontologia e Stratigrafia*, 83, 103–136.

Gelati, R., & Gnaccolini, M. (1978). I conglomerati della Val Borbera, al margine orientale del Bacino terziario ligure-piemontese. *Istituti di Geologia e Paleontologia dell'Università degli Studi di Milano*, 84(3), 701–728.

Ghibaudo, G., Clari, P., & Perello, M. (1985). Litostratigrafia, sedimentologia ed evoluzione tettonico-sedimentaria dei depositi miocenici del margine sud-orientale del bacino terziario ligure-piemontese (Valli Borbera, Scrivia e Lemme). In memoria di Carlo Sturani. *Bollettino Della Società Geologica Italiana*, 104(3), 349–397.

Ghibaudo, G., Massari, F., Chiambretti, I., d'Atri, A., & Fornaciari, E. (2019). Birth and tectono-sedimentary evolution of the Tertiary Piedmont Basin (NW Italy). *Journal of Mediterranean Earth Sciences*, 11, 5–112.

Gholamrezaie, E., Scheck-Wenderoth, M., Sippel, J., & Strecker, M. R. (2018). Variability of the geothermal gradient across two differently aged magma-rich continental rifted margins of the Atlantic Ocean: The Southwest African and the Norwegian margins. *Solid Earth*, 9, 139–158. https://doi.org/10.5194/ se-9-139-2018

Girdler, R. W. (1970). A review of Red Sea heat flow. *Philosophical Transactions of the Royal Society of London*, 267(1181), 191–203.

Gleadow, A. J. W., Duddy, I. R., Green, P. F., & Lovering, J. F. (1986). Confined fission track lengths in apatite: A diagnostic tool for thermal history analysis. *Contributions to Mineralogy and Petrology*, 94(4), 405–415.

Gnaccolini, M., Gelati, R., Falletti, P., & Catrullo, D. (1998). Sequence stratigraphy of the "Langhe" Oligo–Miocene succession, Tertiary Piedmont Basin, northern Italy. In C. P. de Graciansky, J. Hardenbol, T. Jacquin, & P. R. Vail (Eds.), *Mesozoic and Cenozoic sequence stratigraphy of European basins* (pp. 234–244). SEPM Special Publication 60.

Goldstein, R. H. (2001). Fluid inclusions in sedimentary and diagenetic systems. *Lithos*, 55, 159–193. https://doi.org/10.1016/ S0024-4937(00)00044-X

Goldstein, R. H., & Reynolds, T. J. (1994). *Systematics of fluid inclusions in diagenetic minerals* (p. 199). SEPM Short Course 31. https://doi.org/10.2110/scn.94.31

Green, P., & Duddy, I. (2018). Apatite (U-Th-Sm)/He thermochronology on the wrong side of the tracks. *Chemical Geology*, 488, 21–33.

Green, P. F., Duddy, I. R., Laslett, G. M., Hegarty, K. A., Gleadow, A. J. W., & Lovering, J. F. (1989). Thermal annealing of fission tracks in apatite 4. Quantitative modelling techniques and extension to geological timescales. *Chemical Geology: Isotope Geoscience Section*, 79(2), 155–182.

Green, P. F., Duddy, I. R., Gleadow, A. J. W., & Lovering, J. F. (1989). Apatite fission-track analysis as a paleotemperature indicator for hydrocarbon exploration. In *Thermal history of sedimentary basins* (pp. 181–195). Springer.

Gusmeo, T., Cavazza, W., Alania, V. M., Enukidze, O. V., Zattin, M., & Corrado, S. (2021). Structural inversion of back-arc basins—The

Neogene Adjara-Trialeti fold-and-thrust belt (SW Georgia) as a far-field effect of the Arabia-Eurasia collision. *Tectonophysics*, *803*, 228702. https://doi.org/10.1016/j.tecto.2020.228702

Handy, M. R., Schmid, S. M., Bousquet, R., Kissling, E., & Bernoulli, D. (2010). Recoiling plate-tectonic reconstructions of Alpine Tethys with the geological-geophysical record of spreading and subduction in the Alps. *Earth-Science Reviews*, *102*(3), 121–158. https://doi.org/10.1016/j.earscirev.2010.06.002

Handy, M. R., Schmid, S. M., Paffrath, M., Friederich, W., & the AlpArray Working Group. (2021). European tectosphere and slabs beneath the greater Alpine area—Interpretation of mantle 1 structure in the Alps-Apennines-Pannonian region from teleseismic Vp studies. *Solid Earth Discussions*, *2021*, 1–61. https://doi.org/10.5194/se-2021-49

Hurford, A. J. (1990). Standardization of fission track dating calibration: Recommendation by Ficcio Track Working Group of I.U.G.S. Subcommission on Geochronology. *Chemical Geology: Isotope Geoscience Section*, *80*(2), 171–178.

Hurford, A. J., & Green, P. F. (1983). The zeta age calibration of fission-track dating. *Chemical Geology*, *41*, 285–317.

Jamieson, A. R., Beaumont, C., Hamilton, J., & Fullsack, P. (1996). Tectonic assembly of inverted metamorphic sequences. *Geology*, *24*(9), 839. https://doi.org/10.1130/0091-7613(1996)024<0839:TAOIMS>2.3.CO;2

Jolivet, L., & Faccenna, C. (2000). Mediterranean extension and the Africa-Eurasia collision. *Tectonics*, *19*(6), 1095–1106. https://doi.org/10.1029/2000TC900018

Jolivet, L., Gorini, C., Smit, J., & Leroy, S. (2015). Continental break-up and the dynamics of rifting in back-arc basins: The Gulf of Lion margin. *Tectonics*, *34*(4), 662–679. https://doi.org/10.1002/2014TC003570

Kästle, E. D., Rosenberg, C., Boschi, L., Bellahsen, N., Meier, T., & El-Sharkawy, A. (2020). Slab break-offs in the Alpine subduction zone. *International Journal of Earth Sciences (Geologische Rundschau)*, *109*, 587–603. https://doi.org/10.1007/s00531-020-01821-z

Ketcham, R. A. (2005). The role of crystallographic angle in characterizing and modeling apatite fission-track length data. *Radiation Measurements*, *39*(6), 595–601. https://doi.org/10.1016/j.radmeas.2004.07.008

Ketcham, R. A., Carter, A., Donelick, R. A., Barbarand, J., & Hurford, A. J. (2007). Improved modeling of fission-track annealing in apatite. *American Mineralogist*, *92*(5–6), 799–810. https://doi.org/10.2138/am.2007.2281

Ketcham, R. A., Gautheron, C., & Tassan-Got, L. (2011). Accounting for long alpha- particle stopping distances in (U–Th–Sm)/He geochronology: Refinement of the baseline case. *Geochimica et Cosmochimica Acta*, *75*(24), 7779–7791.

Ketcham, R. A., van der Beek, P., Barbarand, J., Bernet, M., & Gautheron, C. (2018). Reproducibility of thermal history reconstruction from apatite fission-track and (U-Th)/He data. *Geochemistry, Geophysics, Geosystems*, *19*(8), 2411–2436.

Kohn, B., Chung, L., & Gleadow, A. (2019). Fission-track analysis: Field collection, sample preparation and data acquisition. In M. Malusà & P. Fitzgerald (Eds.), *Fission-track thermochronology and its application to geology. Springer textbooks in earth sciences, geography and environment*. Springer. https://doi.org/10.1007/978-3-319-89421-8_2

Laubscher, H. P., Biella, G. C., Cassinis, R., Lozey, A., Scarascia, S., & Tobacco, I. (1992). The Ligurian knot. Tethys. *Geologische Rundschau*, *81*, 275–289.

Liao, W. Z., Lin, T. Q., Liu, C. S., Oung, J. N., & Wang, Y. (2014). Heat flow in the rifted continental margin of the South China Sea near Taiwan and its tectonic implications. *Journal of Asian Earth Science*, *92*, 233–244. https://doi.org/10.1016/j.jseaes.2014.01.003

Lippitsch, R., Kissling, E., & Ansorge, J. (2003). Upper mantle structure beneath the Alpine orogen from high-resolution teleseismic tomography. *Journal of Geophysical Research*, *108*(B8), 2376. https://doi.org/10.1029/2002JB002016

Liu, D., Zhao, L., Paul, A., Yuan, H., Solarino, S., Aubert, C., Pondrelli, S., Salimbeni, S., Eva, E., Malusá, M. G., & Guillot, S. (2022). Receiver function mapping of the mantle transition zone beneath the Western Alps: New constraints on slab subduction and mantle upwelling. *Earth and Planetary Science Letters*, *577*, 117267. https://doi.org/10.1016/j.epsl.2021.117267

Luijendik, E., Winter, T., Ferguson, G., von Hagke, C., & Scibek, J. (2020). Using thermal springs to quantify deep groundwater flow and its thermal footprint in the Alps and a comparison with North American orogens. *Geophysical Research Letters*, *47*(22), e2020GL090134.

Macgregor, D. S. (2020). Regional variations in geothermal gradient and heat flow across the African plate. *Journal of African Earth Science*, *171*, 103950.

Maffione, M., Speranza, F., Faccenna, C., Cascella, A., Vignaroli, G., & Sagnotti, L. (2008). A synchronous Alpine and Corsica-Sardinia rotation. *Journal of Geophysical Research: Solid Earth*, *113*, B03104. https://doi.org/10.1029/2007JB005214

Maino, M., Casini, L., Boschi, C., Di Giulio, A., Setti, M., & Seno, S. (2020). Time-dependent heat budget of a thrust from geological records and numerical experiments. *Journal of Geophysical Research: Solid Earth*, *125*, e2019JB018940. https://doi.org/10.1029/2019JB018940

Maino, M., Casini, L., Ceriani, A., Decarlis, A., Di Giulio, A., Seno, S., Setti, M., & Stuart, F. M. (2015). Dating shallow thrusts with zircon (U-Th)/He thermochronometry—The shear heating connection. *Geology*, *43*, 495–498. https://doi.org/10.1130/G36492.1

Maino, M., Dallagiovanna, G., Dobson, K. J., Gaggero, L., Persano, C., Seno, S., & Stuart, F. M. (2012). Testing models of orogen exhumation using zircon (U–Th)/He thermochronology: Insight from the Ligurian Alps, Northern Italy. *Tectonophysics*, *560–561*, 84–93. https://doi.org/10.1016/j.tecto.2012.06.045

Maino, M., Decarlis, A., Felletti, F., & Seno, S. (2013). Tectono-sedimentary evolution of the Tertiary Piedmont Basin (NW Italy) within the Oligo-Miocene central Mediterranean geodynamics. *Tectonics*, *32*(3), 593–619. https://doi.org/10.1002/tect.20047

Maino, M., Gaggero, L., Langone, A., Seno, S., & Fanning, M. (2019). Cambro-Silurian magmatisms at the northern Gondwana margin (Penninic basement of the Ligurian Alps). *Geoscience Frontiers*, *10*(1), 315–330. https://doi.org/10.1016/j.gsf.2018.01.003

Maino, M., & Seno, S. (2016). The thrust zone of the Ligurian Penninic basal contact (Monte Fronté, Ligurian Alps, Italy). *Journal of Maps*, *12*, 341–351. https://doi.org/10.1080/17445647.2016.1213669

Malusà, M. G., Guillot, S., Zhao, L., Paul, A., Solarino, S., Dumont, T., Schwartz, S., Aubert, C., Baccheschi, P., Eva, E., Lu, Y., Lyu, C., Pondrelli, S., Salimbeni, S., Sun, W., & Yuan, H. (2021). The deep structure of the Alps based on the CIFALPS seismic

experiment: A synthesis. *Geochemistry, Geophysics, Geosystems*, *22*(3), e2020GC009466.

Mancin, N., & Pirini, C. (2001). Middle Eocene to early Miocene foraminiferal biostratigraphy in the epiligurian succession (Northern Apennines, Italy). *Rivista Italiana di Paleontologia e Stratigrafia*, *107*(3), 371–393.

Mangenot, X., Bonifacie, M., Gasparrini, M., Götz, A., Chaduteau, C., Ader, M., & Rouchon, V. (2017). Coupling Δ_{47} and fluid inclusion thermometry on carbonate cements to precisely reconstruct the temperature, salinity and $\delta^{18}O$ of paleo-groundwater in sedimentary basins. *Chemical Geology*, *472*, 44–57. https://doi.org/10.1016/j.chemgeo.2017.10.011

Marini, M., Maron, M., Petrizzo, M. R., Felletti, F., & Muttoni, G. (2020). Magnetochronology applied to assess tempo of turbidite deposition: A case study of ponded sheet-like turbidites from the lower Miocene of the northern Apennines (Italy). *Sedimentary Geology*, *403*, 105654. https://doi.org/10.1016/j.sedgeo.2020.105654

Marini, M., Patacci, M., Felletti, F., & McCaffrey, W. D. (2016). Fill to spill stratigraphic evolution of a confined turbidite mini-basin succession, and its likely well bore expression: The Castagnola Fm, NW Italy. *Marine and Petroleum Geology*, *69*, 94–111. https://doi.org/10.1016/j.marpetgeo.2015.10.014

Marroni, M., Feroni, A. C., di Biase, D., Ottria, G., Pandolfi, L., & Taini, A. (2002). Polyphase folding at upper structural levels in the Borbera Valley (northern Apennines, Italy): Implications for the tectonic evolution of the linkage area between Alps and Apennines. *Comptes Rendus Geoscience*, *334*(8), 565–572.

Marroni, M., Meneghini, F., & Pandolfi, L. (2010). International geology review anatomy of the Ligure-Piemontese subduction system: Evidence from late cretaceous-middle Eocene convergent margin deposits in the Northern Apennines, Italy. *International Geology Review*, *52*(10–12), 1160–1192. https://doi.org/10.1080/00206810903545493

Marroni, M., Ottria, G., & Pandolfi, L. (2010). *Note Illustrative della Carta Geologica d'Italia alla scala 1: 50,000 Foglio 196 Cabella Ligure*. Istituto Poligrafico e Zecca Dello Stato.

Mattioli, M., Di Battistini, G., & Zanzucchi, G. (2002). Geochemical features of the Tertiary buried Mortara volcanic body (Northern Apennines, Italy). *Bollettino Della Società Geologica Italiana*, *1*, 239–249.

Mazurek, M., Hurford, A. J., & Leu, W. (2006). Unravelling the multistage burial history of the Swiss Molasse Basin: Integration of apatite fission track, vitrinite reflectance and biomarker isomerisation analysis. *Basin Research*, *18*(1), 27–50.

Midttømme, K., & Roaldset, E. (1999). Thermal conductivity of sedimentary rocks: Uncertainties in measurement and modelling. *Geological Society, London, Special Publications*, *158*, 45–60. https://doi.org/10.1144/GSL.SP.1999.158.01.04

Mitchell, R. K., Indares, A., & Ryan, B. (2014). High to ultrahigh temperature contact metamorphism and dry partial melting of the Tasiuyak paragneiss, northern Labrador. *Journal of Metamorphic Geology*, *32*(6), 535–555. https://doi.org/10.1111/jmg.12086

Mori, H., Mori, N., Wallis, S., Westaway, R., & Annen, C. (2017). The importance of heating duration for Raman CM thermometry: Evidence from contact metamorphism around the Great Whin Sill intrusion, UK. *Journal of Metamorphic Geology*, *35*(2), 165–180. https://doi.org/10.1111/jmg.12225

Mosca, P. (2006). *Neogene basin evolution in the Western Po Plain (NW Italy). Insights from seismic interpretation, subsidence analysis and low temperature (U-Th)/He thermochronology*. [PhD Thesis, Vrije Universiteit, Amsterdam, The Netherlands]. p. 190.

Mosca, P., Polino, R., Rogledi, S., & Rossi, M. (2010). New data for the kinematic interpretation of the Alps–Apennines junction (Northwestern Italy). *International Journal of Earth Sciences*, *99*(4), 833–849.

Mueller, P., Maino, M., & Seno, S. (2020). Progressive deformation patterns from an accretionary prism (Helminthoid Flysch, Ligurian Alps, Italy). *Geosciences*, *10*(1), 26. https://doi.org/10.3390/geosciences10010026

Mutti, E., Papani, L., Di Biase, D., Davoli, G., Mora, S., Segadelli, S., & Tinterri, R. (1995). Il Bacino Terziario Epimesoalpino e le sue implicazioni sui rapporti tra Alpi ed Appennino. *Memorie di Scienze Geologiche di Padova*, *47*, 217–244.

Osadetz, K. G., Kohn, B. P., Feinstein, S., & O'Sullivan, P. B. (2002). Thermal history of Canadian Williston basin from apatite fission-track thermochronology—Implications for petroleum systems and geodynamic history. *Tectonophysics*, *349*(1–4), 221–249.

Pasquale, V., Chiozzi, P., Verdoya, M., & Gola, G. (2012). Heat flow in the Western Po Basin and the surrounding orogenic belts. *Geophysical Journal International*, *190*, 8–22. https://doi.org/10.1111/j.1365-246X.2012.05486.x

Pasquale, V., Gola, G., Chiozzi, P., & Verdoya, M. (2011). Thermophysical properties of the Po Basin rocks. *Geophysical Journal International*, *186*, 69–81.

Patacci, M., Marini, M., Felletti, F., Di Giulio, A., Setti, M., & McCaffrey, W. (2020). Origin of mud in turbidites and hybrid event beds: Insight from ponded mudstone caps of the Castagnola turbidite system (north-west Italy). *Sedimentology*, *67*(5), 2625–2644. https://doi.org/10.1111/sed.12713

Pauselli, C., Gola, G., Mancinelli, P., Trumpy, E., Saccone, M., Manzella, A., & Ranallic, G. (2019, September). A new surface heat flow map of the Northern Apennines between latitudes 42.5 and 44.5 N. *Geothermics*, *81*, 39–52. https://doi.org/10.1016/j.geothermics.2019.04.002

Pieri, M., & Groppi, G. (1981). Subsurface geological structure of the Po Plain, Italy. *Progetto Finalizzato Geodinamica Sottoprogetto "Modello Strutturale", Consiglio Nazionale delle Ricerche*, *414*, 1–13.

Piromallo, C., & Faccenna, C. (2004). How deep can we find the traces of Alpine subduction? *Geophysical Research Letters*, *31*, L06605. https://doi.org/10.1029/2003GL019288

Reiners, P. W., & Brandon, M. T. (2006). Using thermochronology to understand orogenic erosion. *Annual Review of Earth and Planetary Sciences*, *34*(1), 419–466. https://doi.org/10.1146/annurev.earth.34.031405.125202

Reiners, P. W., & Farley, K. A. (2001). Influence of crystal size on apatite (U-Th)/He thermochronology: An example from the Bighorn Mountains, Wyoming. *Earth and Planetary Science Letters*, *188*(3–4), 413–420. https://doi.org/10.1016/S0012-821X(01)00341-7

Reiners, P. W., Spell, T. L., Nicolescu, S., & Zanetti, K. A. (2004). Zircon (U-Th)/He thermochronometry: He diffusion and comparisons with $^{40}Ar/^{39}Ar$ dating. *Geochimica et Cosmochimica Acta*, *68*(8), 1857–1887. https://doi.org/10.1016/j.gca.2003.10.021

Ricci Lucchi, F. (1990). Turbidites in foreland and on-thrust basins of the northern Apennines. *Palaeogeography, Palaeoclimatology, Palaeoecology*, *77*(1), 51–66.

Rollet, N., Déverchère, J., Beslier, M. O., Guennoc, P., Réhault, J. P., Sosson, M., & Truffert, C. (2002). Back arc extension, tectonic inheritance, and volcanism in the Ligurian Sea, Western Mediterranean. *Tectonics*, *21*(3), 6-1–6-23. https://doi.org/10.1029/2001TC900027

Rosenbaum, G., & Lister, G. S. (2005). The Western Alps from the Jurassic to Oligocene: Spatio-temporal constraints and evolutionary reconstructions. *Earth-Science Reviews*, *69*(3–4), 281–306. https://doi.org/10.1016/j.earscirev.2004.10.001

Rossi, M., & Craig, J. (2016). A new perspective on sequence stratigraphy of syn-orogenic basins: Insights from the Tertiary Piedmont Basin (Italy) and implications for play concepts and reservoir heterogeneity. *Geological Society, London, Special Publications*, *436*(1), 93–133.

Rossi, M., Mosca, P., Riccardo, P., Rogledi, S., & Biffi, U. (2009). New outcrop and subsurface data in the Tertiary Piedmont Basin (NW-Italy): Unconformity-bounded stratigraphic units and their relationships with basin-modification phases. *Rivista Italiana di Paleontologia e Stratigrafia*, *115*(3), 305–335.

Ruffini, R., Cosca, M., d'Atri, A., Hunziker, J., & Polino, R. (1995). The volcanic supply of the Taveyanne turbidites (Savoie, France): A riddle for Tertiary Alpine volcanism. *Atti delle Accademia Scienze Roma*, *14*, 359–376.

Salimbeni, S., Agostinetti, N. P., Pondrelli, S., & CIFALPS Working Group. (2021). Insights into the origin and deformation style of the continental Moho: A case-study from the Western Alps (Italy). *Journal of Geophysical Research: Solid Earth*, *126*, e2020JB021319. https://doi.org/10.1029/2020JB021319

Schlunegger, F., & Kissling, E. (2015). Slab rollback orogeny in the Alps and evolution of the Swiss Molasse basin. *Nature Communications*, *6*, 8605. https://doi.org/10.1038/ncomms9605

Schneider, D. A., & Issler, D. R. (2019). Application of low-temperature thermochronology to hydrocarbon exploration. In *Fission-track thermochronology and its application to geology* (pp. 315–333). Springer.

Secchi, G., Casini, L., Cifelli, F., Naitza, S., Carta, E., & Oggiano, G. (2022). Syntectonic magmatism and reactivation of collisional structures during late Variscan shearing (SW Sardinia, Italy). *International Journal of Earth Sciences*, *111*, 1469–1490. https://doi.org/10.1007/s00531-022-02193-2

Séranne, M. (1999). The Gulf of lion continental margin (NW Mediterranean) revisited by IBS: An overview. *Geological Society, London, Special Publications*, *156*(1), 15–36.

Sinclair, H. D. (1997). Flysch to molasse transition in peripheral foreland basins: The role of the passive margin versus slab break-off. *Geology*, *25*, 1123–1126.

Sizova, E., Gerya, T., & Brown, M. (2014). Contrasting styles of Phanerozoic and Precambrian continental collision. *Gondwana Research*, *25*(2), 522–545. https://doi.org/10.1016/j.gr.2012.12.011

Sobel, E. R., & Seward, D. (2010). Influence of etching conditions on apatite fission-track etch pit diameter. *Chemical Geology*, *271*(1), 59–69. https://doi.org/10.1016/j.chemgeo.2009.12.012

Speranza, F., Villa, I. M., Sagnotti, L., Florindo, F., Cosentino, D., Cipollari, P., & Mattei, M. (2002). Age of the Corsica–Sardinia rotation and Liguro–Provençal Basin spreading: New paleomagnetic and Ar/Ar evidence. *Tectonophysics*, *347*(4), 231–251. https://doi.org/10.1016/S0040-1951(02)00031-8

Spooner, C., Scheck-Wenderoth, M., Cacace, M., Götze, H. J., & Luijendijk, E. (2020). The 3D thermal field across the Alpine orogen and its forelands and the relation to seismicity. *Global and Planetary Change*, *193*, 103288. https://doi.org/10.1016/j.gloplacha.2020.103288

Stocchi, S., Cavalli, C., & Baruffini, L. (1992). I depositi torbiditici di Guaso (Pirenei centro meridionali), Gremiasco e Castagnola (settore orientale del BTP): geometria e correlazioni di dettaglio. *Atti Ticinensi Di Scienze Della Terra*, *35*, 153–177.

Tagami, T. (2012). Thermochronological investigation of fault zones. *Tectonophysics*, *538*, 67–85.

Tamburelli, S., Di Giulio, A., Amadori, C., & Consonni, A. (2022). New constraint on burial and thermal history of Devonian reservoir sandstones in the Illizi-Ghadames basin (North Africa) through diagenetic numerical modelling. *Marine and Petroleum Geology*, *145*, 105903. https://doi.org/10.1016/j.marpetgeo.2022.105903

Tang, B., Zhu, C., Qiu, N., Cui, Y., Guo, S., Luo, X., Zhang, B., Li, K., Li, W., & Fu, X. (2021). Analyzing and estimating thermal conductivity of sedimentary rocks from mineral composition and pore property. In *Geofluid in ultra-deep sedimentary basins and their significance for petroleum* (Vol. *2021*, Article ID 6665027, 19 pages). Hindawi Geofluids. https://doi.org/10.1155/2021/6665027

Thybo, H., & Artemieva, I. M. (2013). Moho and magmatic underplating in continental lithosphere. *Tectonophysics*, *609*, 605–619. https://doi.org/10.1016/j.tecto.2013.05.032

Trümpy, R. (1960). Paleotectonic evolution of the central and western Alps. *Bulletin of the Geological Society of America*, *71*, 843–908.

Van Hinte, J. E. (1978). Geohistory analysis-application of micropaleontology in exploration geology. *The American Association of Petroleum Geologists Bulletin*, *62*(2), 201–222.

Vance, J. A. (1999). Zircon fission track evidence for a Jurassic (Tethyan) thermal event in the Western Alps. *Memorie di Scienze Geologiche Padova*, *51*(2), 473–476.

Vanossi, M., Cortesogno, L., Galbiati, B., Messiga, B., Piccardo, G. B., & Vannucci, R. (1986). Geologia delle Alpi Liguri: dati, problemi, ipotesi. *Mémoires de la Société géologique de Italiana*, *28*, 5–75.

Vanossi, M., Perotti, C. R., & Seno, S. (1994). The maritime alps arc in the ligurian and tyrrhenian systems. *Tectonophysics*, *230*(1–2), 75–89. https://doi.org/10.1016/0040-1951(94)90147-3

Vedova, B. D., Bellani, S., Pellis, G., & Squarci, P. (2001). Deep temperatures and surface heat flow distribution. In G. B. Vai & I. P. Martini (Eds.), *Anatomy of an orogen: the apennines and adjacent mediterranean basins*. Springer. https://doi.org/10.1007/978-94-015-9829-3_7

Vermeesch, P. (2012). On the visualisation of detrital age distributions. *Chemical Geology*, *312–313*, 190–194. https://doi.org/10.1016/j.chemgeo.2012.04.021

Vignaroli, G., Faccenna, C., Jolivet, L., Piromallo, C., & Rossetti, F. (2008). Subduction polarity reversal at the junction between the Western Alps and the northern Apennines, Italy. *Tectonophysics*, *450*(1–4), 34–50. https://doi.org/10.1016/j.tecto.2007.12.012

Vignaroli, G., Rossetti, F., Rubatto, D., Theye, T., Lisker, F., & Phillips, D. (2010). Pressure-temperature-deformation-time (P-T-d-t) exhumation history of the Voltri Massif HP complex, Ligurian Alps, Italy. *Tectonics*, *29*, TC6009. https://doi.org/10.1029/2009TC002621

von Blanckenburg, F., & Davies, J. H. (1995). Slab breakoff: A model for syncollisional magmatism and tectonics in the Alps. *Tectonics*, *14*, 120–131.

Vosteen, H. D., & Schellschmidt, R. (2003). Influence of temperature on thermal conductivity, thermal capacity and thermal diffusivity for different types of rock. *Physics and Chemistry of the Earth*, *28*, 499–509.

Whittington, A. G., Hofmeister, A. M., & Nabelek, P. I. (2009). Temperature-dependent thermal diffusivity of the Earth's crust and implication for magmatism. *Nature*, *458*, 319–321. https://doi.org/10.1038/nature07818

Wildman, M., Brown, R., Persano, C., Beucher, R., Stuart, F. M., Mackintosh, V., Gallagher, K., Schwanethal, J., & Carter, A. (2017). Contrasting Mesozoic evolution across the boundary between on and off craton regions of the South African plateau inferred from apatite fission track and (U-Th-Sm)/He thermochronology. *Journal of Geophysical Research - Solid Earth*, *122*, 1517–1547. https://doi.org/10.1002/2016JB013478

Yalçin, M. N., Littke, R., & Sachsenhofer, R. F. (1997). Thermal history of sedimentary basins. In D. H. Welte, B. Horsfield, & D. R. Baker (Eds.), *Petroleum and basin evolution*. Springer. https://doi.org/10.1007/978-3-642-60423-2_3

Yalçin, M. N., & Welte, D. H. (1988). The thermal evolution of sedimentary basins and significance for hydrocarbon generation. *Bulletin of Turkish Petroleum Geology, Ankara*, *1*, 12–26.

Zattin, M., Landuzzi, A., Picotti, V., & Zuffa, G. G. (2000). Discriminating between tectonic and sedimentary burial in a foredeep succession, northern Apennines. *Journal of the Geological Society*, *157*, 629–633.

Ziegler, P. A., & Dèzes, P. (2006). Crustal evolution of western and Central Europe. *Geological Society, London, Memoirs*, *32*(1), 43–56.

SUPPORTING INFORMATION

Additional supporting information can be found online in the Supporting Information section at the end of this article.